Particle Accelerators, 1997, Vol. 57, pp. 9–64
Reprints available directly from the publisher
Photocopying permitted by license only

LONGITUDINAL WAKEFIELD FOR AN ELECTRON MOVING ON A CIRCULAR ORBIT

J.B. MURPHY [a,*], S. KRINSKY [a] and R.L. GLUCKSTERN [b]

[a] *National Synchrotron Light Source, Brookhaven National Laboratory, Upton, NY 11973, USA;* [b] *Physics Department, University of Maryland, College Park, MD 20742, USA*

(Received 6 May 1996; Revised 28 January 1997; In final form 10 March 1997)

Using a time-domain analysis, we determine the longitudinal wakefield of an electron moving on a circular orbit in both free space, and between a pair of symmetrically placed infinitely conducting plates. Our calculation is restricted to points on the circular orbit. We obtain an analytic expression for the short-range wakefield of a highly relativistic electron in free space. For an electron circulating midway between parallel plates, the method of image charges is used to derive the wakefield, exhibit a scaling property and evaluate the scaling functions. As a complement to the time-domain analysis of the wakefield, we discuss its frequency-domain counterpart, the longitudinal coupling impedance. Beginning with a review of the seminal work of Schott from the early part of the century, our presentation continues to the frontier where many new results are provided.

Keywords: Synchrotron radiation; Wakefield; Impedance

1. INTRODUCTION

It is of interest to determine how short a bunch can be maintained in a storage ring. Can 10^7–10^8 electrons be stored in a bunch of rms length 300, 100, 50 μm, ...? Some aspects of this problem depend on specific details of the storage ring design. A question of more universal character is whether the curvature wakefield, resulting from synchrotron radiation, can result in bunch lengthening. This has been discussed for a long time, but there is still no definitive answer.

* Corresponding author. Tel.: 516 344 5160. E-mail: jbm@bnl.gov.

In this paper, we present a detailed discussion of the longitudinal wakefield due to orbit curvature. Motivated by the pioneering work of Schott,[1] published in 1912, we focus on the time-domain description of the radiation field, although the impedance is also discussed. Part of this paper is a review, since we treat aspects of the problem already discussed in the literature.[1–16] However, new results are also presented. We derive a simple analytic expression for the short-range wakefield of a highly relativistic electron in free space. Also, using the method of images, we determine the wakefield for an electron moving on a circular trajectory between two parallel plates of infinite conductivity. A short account of some of the results we have obtained was presented in Ref. 17.

Our study identifies the parameter $\Sigma \equiv (\sigma/(2\rho))(\rho/h)^{3/2}$, Eq. (8.8), as the key to determining whether or not the wakefield of a Gaussian bunch of length σ, circulating in a magnet of bending radius ρ, is affected by infinite extent conducting plates located a distance $\pm h$ above or below the electron beam. For $\Sigma \ll 1$, the plates produce a negligible effect on the free space wakefield on a scale length of order of a few σ. Therefore, we suggest that in the determination of the equilibrium bunch length of very short bunches, the effect of the conducting plates can be neglected and the starting point for bunch lengthening calculation should be the free space wakefield. As Σ increases beyond 0.2 the free space results begin to be modified by the shielding plates.

In Section 2, we review the result of Schott for the electromagnetic field at all points on the circular orbit of the radiating electron. In Section 3, we utilize this result to determine an analytic expression for the wakefield of a highly relativistic electron moving in free space. See Eqs. (3.10)–(3.16) and Figure 2. This extends previous work in Refs. 5, 8, and 12. In Section 4, the problem of an electron moving on a circular orbit between parallel plates is treated in the time-domain utilizing the method of image charges. Previous work on this problem[3,5,7,11,13–16] has all been in the frequency domain. The solution found in Section 4 is considered in greater detail in Section 5. A scaling property of the wakefield is exhibited, and the scaling functions are evaluated. See Eq. (5.21) and Figure 3. The behavior of the wakefield is considered for large distances (times). In free space, the wakefield has an algebraic fall off for large distances (times), but in

the presence of the conducting plates, this algebraic fall off is cancelled by the fields due to the image charges, resulting in an exponential decay of the wakefield, as expressed in Eq. (5.34). This is the time-domain analog of the suppression of low frequencies in the resistive impedance due to the parallel plates. The impedance in free space is discussed in Section 6, and between parallel plates in Section 7. The coherent power radiated between parallel plates is considered in Section 8. The wakefield resulting from a bunch of electrons is discussed in Section 9. Some concluding remarks are given in Section 10. In the appendices, we derive from the wakefield, representations for the impedance in free space (Appendix A) and between parallel plates (Appendix B). In Appendix C, we present numerical results, illustrating the important scaling property of the wakefield between parallel plates derived in Section 5.1.

2. REVIEW OF SCHOTT'S RESULT

In his pioneering book, *Electromagnetic Radiation*, published in 1912, Schott[1] calculated many of the properties of the radiation due to a relativistic point charge moving with uniform velocity on a circular orbit. In particular, Schott determined the electromagnetic field at all points on the circular orbit, yielding what we now refer to as the wakefield of the point charge. Here, it is our goal to extend Schott's work in several directions, considering a highly relativistic particle whose velocity is close to the speed of light c. In this case the longitudinal wakefield is large in front of the point charge and very small behind. Working directly in the time domain, we first obtain a simple analytic expression for this leading longitudinal wake. Next, we use the method of image charges to derive the longitudinal wake due to a point charge moving on a circular orbit lying between two parallel plates of infinite conductivity.

The Liénard–Wiechert potentials and fields for a point particle are derivable from the time-dependent Green's function[2,18]

$$G(\vec{x}, t; \vec{x}', t') = \frac{\delta(t' - t + |\vec{x} - \vec{x}'|/c)}{|\vec{x} - \vec{x}'|}. \tag{2.1}$$

In the Lorentz gauge, the scalar and vector potentials are given by

$$\Phi(\vec{x}, t) = \int \mathrm{d}^3x'\mathrm{d}t'\rho(\vec{x}', t')G(\vec{x}, t; \vec{x}', t'), \tag{2.2a}$$

$$\vec{A}(\vec{x}, t) = \int \mathrm{d}^3x'\mathrm{d}t'\vec{j}(\vec{x}', t')G(\vec{x}, t; \vec{x}', t'). \tag{2.2b}$$

For a point particle following a trajectory $\vec{r}_0(t)$, the charge density and current density are

$$\rho(\vec{x}, t) = e\delta(\vec{x} - \vec{r}_0(t)), \tag{2.3a}$$

$$\vec{j}(\vec{x}, t) = \vec{v}_0(t)\rho(\vec{x}, t), \tag{2.3b}$$

where $\vec{v}_0(t) = c\vec{\beta}_0(t) = \mathrm{d}\vec{r}_0(t)/\mathrm{d}t$ is the instantaneous velocity. The Liénard–Wiechert potentials are

$$\Phi(\vec{x}, t) = \frac{e}{|\vec{x} - \vec{r}_0(\tau)| - \vec{\beta}_0(\tau) \cdot (\vec{x} - \vec{r}_0(\tau))}, \tag{2.4a}$$

$$\vec{A}(\vec{x}, t) = \frac{e\vec{\beta}_0(\tau)}{|\vec{x} - \vec{r}_0(\tau)| - \vec{\beta}_0(\tau) \cdot (\vec{x} - \vec{r}_0(\tau))}. \tag{2.4b}$$

The retarded time τ is defined by the implicit equation

$$\tau = t - \frac{|\vec{x} - \vec{r}_0(\tau)|}{c}. \tag{2.5}$$

Following Schott,[1] in Figure 1 we introduce the angle 2χ between the observation point $\vec{x}$ (at time t) and the emission point $\vec{x}' = \vec{r}_0(\tau)$ at the retarded time. Note that in Figure 1 the observation point lies behind the source point. It is seen that in the plane of the circular orbit,

$$|\vec{x} - \vec{r}_0(\tau)| = 2\rho \sin \chi(\tau), \tag{2.6}$$

where ρ is the radius of the circular orbit; hence

$$\Phi(\vec{x}, t) = \frac{1}{2\rho \sin \chi(\tau)} \frac{e}{1 + \beta \cos \chi(\tau)}, \tag{2.7a}$$

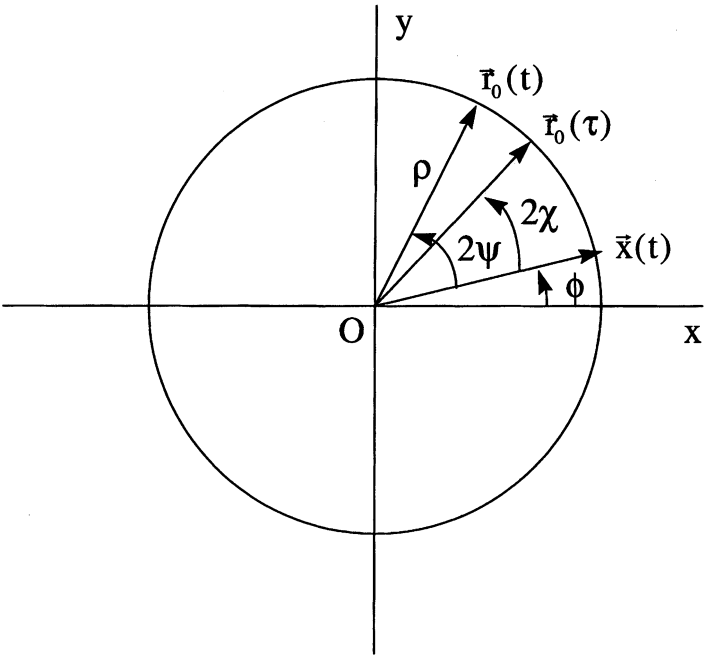

FIGURE 1 Geometry for an electron moving on a circular orbit of radius ρ. 2χ is the angle between the observation point $\vec{x}(t)$ at the time t, and the emission point $\vec{r}_0(\tau)$ at the retarded time τ. Note that the observation point lies behind the source point. 2ψ is the angle between the observation point $\vec{x}(t)$ at the time t, and the present position $\vec{r}_0(t)$ of the electron at time t.

$$A_\phi(\vec{x}, t) = \frac{1}{2\rho \sin \chi(\tau)} \frac{e\beta(1 - 2\sin^2 \chi(\tau))}{1 + \beta \cos \chi(\tau)}. \tag{2.7b}$$

Here, A_ϕ is the component of the vector potential tangent to the circular orbit at the observation point $\vec{x}$. In Figure 1, we also introduce the angle 2ψ between the observation point $\vec{x}$ (at time t) and the present position $\vec{r}_0(t)$ of the electron. Clearly

$$2\psi - 2\chi = \omega_0(t - \tau), \tag{2.8}$$

where the angular frequency $\omega_0 = \beta c/\rho$. Utilizing Eqs. (2.5), (2.6) and (2.8) we derive the retardation condition

$$\psi = \chi + \beta \sin \chi. \tag{2.9}$$

In the notation of Schott,[1] the trajectory of the electron in the plane is parametrized according to

$$\vec{r}_0(t) = (\rho\cos(\omega_0 t + \delta), \rho\sin(\omega_0 t + \delta)), \tag{2.10}$$

where δ is a constant phase. The observation point $\vec{x}$ is specified by

$$\vec{x} = (\rho\cos\phi, \rho\sin\phi). \tag{2.11}$$

Schott writes

$$\chi = \frac{1}{2}(\omega_0\tau + \delta - \phi), \tag{2.12a}$$

$$\psi = \frac{1}{2}(\omega_0 t + \delta - \phi), \tag{2.12b}$$

from which we see that

$$\frac{\partial}{\partial\phi} = -\frac{1}{2}\frac{\partial}{\partial\psi}, \tag{2.13a}$$

$$\frac{\partial}{\partial t} = \frac{\omega_0}{2}\frac{\partial}{\partial\psi} = \frac{c\beta}{2\rho}\frac{\partial}{\partial\psi}. \tag{2.13b}$$

The tangential electric field at the observation point is

$$E_\phi = -\frac{1}{\rho}\frac{\partial}{\partial\phi}\Phi(\vec{x}, t) - \frac{1}{c}\frac{\partial}{\partial t}A_\phi. \tag{2.14}$$

Employing Eqs. (2.12) and (2.13) one derives Schott's[1] result

$$E_\phi = \frac{\partial}{\partial\psi}\left[\frac{e}{4\rho^2\sin\chi}\frac{1-\beta^2}{1+\beta\cos\chi} + \frac{e}{2\rho^2}\frac{\beta^2\sin\chi}{1+\beta\cos\chi}\right]. \tag{2.15}$$

Note that for motion in the plane, as considered here, the field is expressable as the gradient of a "potential." Recall that χ is determined as a function of ψ by the retardation condition of Eq. (2.9).

The trailing wake, behind the point charge, corresponds to $\chi \sim 0$ and $\psi \sim 0$. The factor $1+\beta\cos\chi$ in the denominator is approximately equal to two, and the trailing wake is not large. The leading

wake, in front of the electron, corresponds to $\chi \sim \pi$ and $\psi \sim \pi$. Now the factor $1+\beta\cos\chi$ in the denominator is close to vanishing when $\beta \sim 1$, hence the leading wake is much larger than the trailing wake for a highly relativistic particle.

Starting from the expression for E_ϕ given in Eq. (2.15), Schott separated the singular Coulomb term, and carried out a Fourier expansion in the variable ψ for the non-singular contribution to E_ϕ due to synchrotron radiation, obtaining

$$E_\phi = -\frac{e(1-\beta^2)\cos\psi}{4\rho^2\sin^2\psi} - \frac{e}{\rho^2}\sum_{m=1}^{\infty}(-1)^m \cos m\psi \times \left[m\beta^2 J'_m(m\beta) - \frac{1}{2}(1-\beta^2)m^2\int_0^\beta J_m(mx)\,\mathrm{d}x\right]. \tag{2.16}$$

3. FREE SPACE WAKEFIELD

In considering the leading wake of a highly relativistic electron, it is convenient to introduce the angles α and ξ according to

$$\psi = \pi - \xi, \tag{3.1a}$$

$$\chi = \pi - \alpha. \tag{3.1b}$$

Equation (2.15) can then be written as

$$E_\phi = -\frac{\partial V}{\partial \xi}, \tag{3.2a}$$

$$V = \frac{e}{2\rho^2}\left[\frac{1-\beta^2}{2\sin\alpha\,(1-\beta\cos\alpha)} + \frac{\beta^2\sin\alpha}{1-\beta\cos\alpha}\right], \tag{3.2b}$$

where α is determined as a function of ξ by the retardation condition of Eq. (2.9):

$$\xi = \alpha - \beta\sin\alpha. \tag{3.3}$$

For the short-range leading wake, the angles ξ and α are small, so Eq. (3.3) can be simplified using $\sin\alpha \cong \alpha - \alpha^3/6$. We consider a highly relativistic electron for which $\gamma = (1-\beta^2)^{-1/2}$ is large, and

replace Eq. (3.3) by the approximate equality

$$\alpha^3 + \frac{3}{\gamma^2}\alpha - 6\xi = 0. \tag{3.4}$$

The solution of this cubic equation for α, which vanishes when ξ approaches zero, is given by

$$\gamma\alpha = \Omega^{1/3} - \Omega^{-1/3}, \tag{3.5}$$

where

$$\Omega = \mu + \sqrt{\mu^2 + 1} \tag{3.6a}$$

and

$$\mu = 3\gamma^3\xi = n_c s/\rho. \tag{3.6b}$$

Here s is the arc length between the charge and the observation point, and $n_c = 3\gamma^3/2$.

In Eq. (3.2b), let us separate the singular Coulomb term

$$V = \frac{e}{2\rho^2}\left[\frac{1-\beta^2}{2\sin\xi} + F\right], \tag{3.7a}$$

$$F = \frac{1-\beta^2}{2\sin\alpha\,(1-\beta\cos\alpha)} + \frac{\beta^2\sin\alpha}{1-\beta\cos\alpha} - \frac{1-\beta^2}{2\sin\xi}. \tag{3.7b}$$

The expression for the non-singular radiation contribution to the wakefield can be reduced using small angle approximations to the form

$$\frac{F}{\gamma} = \frac{1}{\gamma\alpha(1+\gamma^2\alpha^2)} + \frac{2\gamma\alpha}{1+\gamma^2\alpha^2} - \frac{3}{2\mu}, \tag{3.8}$$

and using Eq. (3.6) one can show

$$\frac{F}{\gamma} = \frac{-1}{\mu} + \frac{2(\Omega^{1/3} + \Omega^{-1/3})}{(\Omega - \Omega^{-1})(\Omega + \Omega^{-1})} + \frac{2(\Omega^{2/3} - \Omega^{-2/3})}{\Omega + \Omega^{-1}}. \tag{3.9}$$

Let us write the tangential electric field as a sum of the singular Coulomb term and a non-singular term $\tilde{E}_\phi$ due to synchrotron radiation:

$$E_\phi = \frac{-e(1-\beta^2)\cos\psi}{4\rho^2 \sin^2\psi} + \tilde{E}_\phi. \tag{3.10}$$

We now write, for $\mu > 0$,

$$\tilde{E}_\phi = -\frac{4}{3}\frac{e\gamma^4}{\rho^2} w(\mu), \tag{3.11}$$

where

$$w(\mu) = \frac{\mathrm{d}v(\mu)}{\mathrm{d}\mu}, \tag{3.12}$$

and

$$\begin{aligned} v(\mu) &= \frac{9}{8}\frac{F}{\gamma} \\ &= \frac{9}{16}\left\{\frac{-2}{\mu} + \frac{1}{\mu\lambda}\left[(\lambda+\mu)^{1/3} + (\lambda+\mu)^{-1/3}\right]\right. \\ &\quad \left. + \frac{2}{\lambda}\left[(\lambda+\mu)^{2/3} - (\lambda+\mu)^{-2/3}\right]\right\}, \end{aligned} \tag{3.13}$$

with $\lambda = \sqrt{\mu^2+1}$. The expression for $v(\mu)$ can be simplified by introducing the parametrization

$$\mu = \sinh\eta. \tag{3.14}$$

It is easily verified that for $\mu > 0$,

$$v(\mu) = \frac{9}{4}\,\frac{\cosh\left[\frac{5}{3}\sinh^{-1}\mu\right] - \cosh\left[\sinh^{-1}\mu\right]}{\sinh\left[2\sinh^{-1}\mu\right]}. \tag{3.15}$$

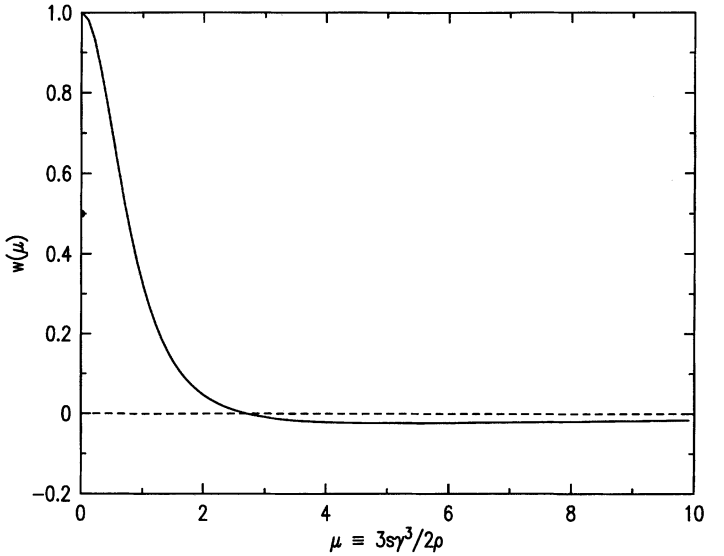

FIGURE 2 Plot of the free space wake function $w(\mu)$ versus μ as given by Eqs. (3.12) and (3.15).

The function $w(\mu)$ is plotted in Figure 2. Some useful properties of $w(\mu)$ are

$$w(\mu) = \begin{cases} 1 - \dfrac{14}{9}\mu^2 + \cdots, & \mu^2 \ll 1, \\ -\dfrac{3}{4 \cdot 2^{1/3}} \dfrac{1}{\mu^{4/3}} + \cdots, & \mu^2 \gg 1, \\ \dfrac{1}{2}, & \mu = 0, \\ 0, & \mu < 0. \end{cases} \tag{3.16}$$

The wakefield behind the charge is of order $1/\gamma^4$ smaller than that just in front of it. The asymptotic expansions for large and small μ were discussed previously in Refs. 5, 8, and 12. Noting that $v(\mu)$ vanishes at $\mu = 0$ and $\mu = \infty$, it follows from Eq. (3.12) that

$$\int_0^\infty w(\mu)\, d\mu = 0. \tag{3.17}$$

The wake function is discontinuous at the position of the point charge. The choice $w(0) = \frac{1}{2}$ represents an average of the electric field

immediately in front and behind the charge, and results in the power loss being correctly given by $ec\beta E_\phi(0)$. The total power radiated by N particles is

$$P = \frac{4}{3}\frac{ce^2\gamma^4}{\rho^2}\left[\frac{N}{2} + \sum_{p>q} w(\mu_p - \mu_q)\right]. \tag{3.18}$$

The double sum can be approximated by an integral by introducing the number density $n(\mu_p)$, with the normalization

$$\int_{-\infty}^{\infty} \mathrm{d}\mu_p\, n(\mu_p) = 1. \tag{3.19}$$

Onẽ then finds

$$\sum_{p>q} w(\mu_p - \mu_q) \approx N^2 \int_{-\infty}^{\infty} \mathrm{d}\mu_p\, n(\mu_p) \int_{-\infty}^{\mu_p} \mathrm{d}\mu_q\, n(\mu_q) w(\mu_p - \mu_q). \tag{3.20}$$

Carrying out some straightforward manipulation of this integral and an integration by parts, we can write ($\beta = 1$)

$$P = \frac{4}{3}\frac{ce^2\gamma^4}{\rho^2}\left[\frac{N}{2} + N^2 C\right], \tag{3.21}$$

where

$$C = \int_{-\infty}^{\infty} \mathrm{d}\mu\, n(\mu) \int_0^{\infty} \mathrm{d}\lambda\, n'(\mu - \lambda) v(\lambda), \tag{3.22}$$

and $v(\lambda)$ was defined in Eq. (3.12).

For a rectangular density profile

$$n_{\mathrm{R}}(\mu) = \begin{cases} \dfrac{1}{2\mu_0}, & |\mu| < \mu_0, \\ 0, & |\mu| > \mu_0, \end{cases} \tag{3.23}$$

one finds

$$C = \frac{1}{4\mu_0^2} \int_0^{2\mu_0} \mathrm{d}\zeta\, v(\zeta), \tag{3.24}$$

and for a Gaussian distribution

$$n_G(\mu) = \frac{1}{\sigma_\mu \sqrt{2\pi}} e^{-\mu^2/2\sigma_\mu^2}, \tag{3.25}$$

it follows that

$$C = \frac{1}{4\sigma_\mu^3 \sqrt{\pi}} \int_0^\infty d\zeta\, \zeta v(\zeta) e^{-\zeta^2/4\sigma_\mu^2}. \tag{3.26}$$

In Eqs. (3.24) and (3.26), when the bunch length is large compared to ρ/γ^3, the large argument approximation for $v(\zeta)$ can be used:

$$v(\zeta) \approx \frac{9}{4 \cdot 2^{1/3}} \zeta^{-1/3}, \quad \zeta^2 \gg 1. \tag{3.27}$$

Evaluating the integrals in Eqs. (3.24) and (3.26) using (3.27), we derive

$$P = \frac{4}{3} \frac{ce^2\gamma^4}{\rho^2} \left[\frac{N}{2} + \frac{3}{4} N^2 B \left(\frac{\rho/\gamma^3}{2\sigma_\ell} \right)^{4/3} \right]. \tag{3.28}$$

Here, $B = 1$ for the rectangular distribution and $B = 2\Gamma(5/6)/3^{1/3}\sqrt{\pi} \approx 0.88$ for the Gaussian distribution. We use σ_ℓ to denote the rms bunch length in each case. For the rectangular distribution, $\mu_0 = 3\gamma^3\sqrt{3}\sigma_\ell/2\rho$ and for the Gaussian distribution $\sigma_\mu = 3\gamma^3\sigma_\ell/2\rho$, recalling the definition of μ in Eq. (3.6b).

For a Gaussian bunch, Eq. (3.28) is in agreement with the result of Schiff,[3] and for a rectangular bunch with the result of Nodvick and Saxon.[3] The result presented by Nodvick and Saxon for the case of a Gaussian bunch appears to be too large by a factor $2^{5/3}$.

4. SOLUTION BETWEEN PARALLEL PLATES USING IMAGE CHARGES

Let us now consider an electron moving with uniform velocity on a circular orbit in the horizontal midplane between two parallel plates

of infinite conductivity located at $z = \pm h$. Using the method of image charges we easily see that the free space Green's function of Eq. (2.1) should be replaced by the parallel plate Green's function

$$G_{\mathrm{pp}}(\vec{x}, t; \vec{x}', t') = \sum_{k=-\infty}^{\infty} \frac{(-1)^k \delta(t' - t + |\vec{x} - \vec{x}' - 2kh\hat{z}|/c)}{|\vec{x} - \vec{x}' - 2kh\hat{z}|}. \tag{4.1}$$

Here the observation point $\vec{x}$ and the source point $\vec{x}'$ lie in the midplane, and $\hat{z}$ is a unit vector in the vertical direction perpendicular to the plates. This approach working in the time domain complements earlier work utilizing the frequency domain.[3,5,7,11,13–16]

As in Section 2, the electron trajectory in the midplane is denoted $\vec{r}_0(t)$, and the charge density and current density are specified by Eq. (2.3). Using Eq. (2.2) with the Green's function of Eq. (4.1), we determine the scalar and vector potentials in the case of parallel plates:

$$\Phi(\vec{x}, t) = \sum_{k=-\infty}^{\infty} \frac{(-1)^k e}{|\vec{x} - \vec{r}_0(\tau_k) - 2kh\hat{z}| - \vec{\beta}_0(\tau_k) \cdot (\vec{x} - \vec{r}_0(\tau_k))}, \tag{4.2a}$$

$$\vec{A}(\vec{x}, t) = \sum_{k=-\infty}^{\infty} \frac{(-1)^k e \vec{\beta}_0(\tau_k)}{|\vec{x} - \vec{r}_0(\tau_k) - 2kh\hat{z}| - \vec{\beta}_0(\tau_k) \cdot (\vec{x} - \vec{r}_0(\tau_k))}. \tag{4.2b}$$

The retarded time τ_k corresponding to the kth image charge is determined by

$$\tau_k = t - \frac{|\vec{x} - \vec{r}_0(\tau_k) - 2kh\hat{z}|}{c}. \tag{4.3}$$

Proceeding as in Section 2, we introduce the angle $2\chi_k$ between the observation point $\vec{x}$ (at time t) and the emission point $\vec{x}' = \vec{r}_0(\tau_k)$ at the retarded time τ_k [Eq. (4.3)] for the kth image charge. Clearly,

$$|\vec{x} - \vec{r}_0(\tau_k)| = 2\rho \sin \chi_k, \tag{4.4a}$$

$$|\vec{x} - \vec{r}_0(\tau_k) - 2kh\hat{z}| = \sqrt{(2\rho \sin \chi_k)^2 + (2kh)^2}, \tag{4.4b}$$

$$\vec{\beta}_0(\tau_k) \cdot \hat{z} = 0. \tag{4.4c}$$

It follows that

$$\Phi(\vec{x},t)=\sum_{k=-\infty}^{\infty}\frac{(-1)^k e}{\sqrt{(2\rho\sin\chi_k)^2+(2kh)^2}+\beta(2\rho\sin\chi_k)\cos\chi_k}, \tag{4.5a}$$

$$A_\phi(\vec{x},t)=\sum_{k=-\infty}^{\infty}\frac{(-1)^k e\beta(1-2\sin^2\chi_k)}{\sqrt{(2\rho\sin\chi_k)^2+(2kh)^2}+\beta(2\rho\sin\chi_k)\cos\chi_k}. \tag{4.5b}$$

We also introduce the angle 2ψ between the observation point $\vec{x}$ (at the time t) and the present position $\vec{r}_0(t)$ of the electron. In a manner analogous to the derivation of Eq. (2.8), one can show that the angle χ_k is determined as a function of ψ by the retardation condition:

$$\psi=\chi_k+\frac{\beta}{2\rho}\sqrt{(2\rho\sin\chi_k)^2+(2kh)^2}. \tag{4.6}$$

The tangential electric field can now be determined from Eqs. (2.12) and (2.13) which imply

$$E_\phi=\frac{1}{2\rho}\frac{\partial}{\partial\psi}(\Phi-\beta A_\phi); \tag{4.7}$$

hence

$$E_\phi(\vec{x},t)=\frac{\partial}{\partial\psi}\sum_{k=-\infty}^{\infty}(-1)^k\left[\frac{e}{2\rho}\frac{1-\beta^2}{\sqrt{(2\rho\sin\chi_k)^2+(2kh)^2}+\beta(2\rho\sin\chi_k)\cos\chi_k}\right.$$
$$\left.+\frac{e}{\rho}\frac{\beta^2\sin^2\chi_k}{\sqrt{(2\rho\sin\chi_k)^2+(2kh)^2}+\beta(2\rho\sin\chi_k)\cos\chi_k}\right], \tag{4.8}$$

where Eq. (4.6) is used to express χ_k as a function of ψ.

5. WAKEFIELD BETWEEN PARALLEL PLATES

5.1. Scaling Property of the Wakefield

We are now able to determine the wakefield of a highly relativistic electron moving on a circular orbit in the midplane between two

parallel plates of infinite conductivity. Defining the angles ξ and α_k by

$$\psi = \pi - \xi, \tag{5.1a}$$

$$\chi_k = \pi - \alpha_k, \tag{5.1b}$$

Eq. (4.8) can be written in the form

$$E_\phi = -\frac{\partial}{\partial \xi} \sum_{k=-\infty}^{\infty} (-1)^k \left[\frac{e(1-\beta^2)}{4\rho^2} V_{1,k} + \frac{e\beta^2}{2\rho^2} V_{2,k} \right], \tag{5.2}$$

where

$$V_{1,k} = \frac{1}{s_k - (\beta/2)\sin 2\alpha_k}, \tag{5.3a}$$

$$V_{2,k} = \frac{\sin^2 \alpha_k}{s_k - (\beta/2)\sin 2\alpha_k}, \tag{5.3b}$$

$$s_k = \sqrt{\sin^2 \alpha_k + (kh/\rho)^2}. \tag{5.4}$$

The angle α_k is determined as a function of ξ by the retardation condition

$$\xi = \alpha_k - \beta\sqrt{\sin^2 \alpha_k + k^2\Delta^2}, \tag{5.5}$$

where we have defined

$$\Delta = h/\rho. \tag{5.6}$$

In treating the contributions from the image charges ($k \neq 0$), we assume $\gamma^2\Delta \gg 1$ and set $\beta = 1$ in Eq. (5.5).

In what follows we shall consider the dominant contribution of the parallel plates to the wakefield given in Eq. (5.2). This contribution arises from the low k terms in the sum on k for which the solution of Eq. (5.5) satisfies the criteria that $\alpha_k \leq 1$. It can be shown that

the remainder of the terms in the infinite sum over k give a small contribution to the wakefield. Proceeding under the assumption $\alpha_k \leq 1$, Eq. (5.5) can be approximated by

$$\xi^2 - 2\alpha_k \xi \cong k^2\Delta^2 - \alpha_k^4/3. \tag{5.7}$$

We now exploit a scaling property of the wake function due to image charges (for $\Delta \ll 1$) by defining the variables x and y_k via

$$\alpha_k = y_k(k\Delta)^{1/2}, \tag{5.8a}$$

$$\xi = x\Delta^{3/2}. \tag{5.8b}$$

Keeping only terms of order Δ^2, Eq. (5.7) reduces to

$$\frac{x}{k^{3/2}} = \frac{y_k^3}{6} - \frac{1}{2y_k}. \tag{5.9}$$

From Eq. (5.3a), we find

$$V_{1,k} \cong \frac{1}{s_k - \alpha_k + \frac{2}{3}\alpha_k^3}. \tag{5.10}$$

The retardation condition of Eq. (5.5) tells us that $s_k - \alpha_k = -\xi$ (when $\beta = 1$). Therefore, using Eqs. (5.8) and (5.9) we obtain

$$V_{1,k} \cong \frac{2}{(k\Delta)^{3/2}} \frac{y_k}{1 + y_k^4}. \tag{5.11}$$

In a similar manner one finds from Eq. (5.3b)

$$V_{2,k} \cong \frac{2}{(k\Delta)^{1/2}} \frac{y_k^3}{1 + y_k^4}. \tag{5.12}$$

Since

$$\frac{\partial V}{\partial \xi} = \frac{1}{\Delta^{3/2}} \frac{\partial V}{\partial x} = \frac{1}{\Delta^{3/2}} \frac{\partial V}{\partial y_k} \frac{\partial y_k}{\partial x}, \tag{5.13a}$$

and

$$\frac{\partial y_k}{\partial x} = \frac{2y_k^2}{1+y_k^4} \cdot \frac{1}{k^{3/2}}, \tag{5.13b}$$

we conclude

$$\frac{\partial V_{1,k}}{\partial \xi} = \frac{4}{(k\Delta)^3} \frac{y_k^2(1-3y_k^4)}{(1+y_k^4)^3} \tag{5.14a}$$

and

$$\frac{\partial V_{2,k}}{\partial \xi} = \frac{4}{(k\Delta)^2} \frac{y_k^4(3-y_k^4)}{(1+y_k^4)^3}, \tag{5.14b}$$

where y_k is determined as a function of $x/k^{3/2}$ by Eq. (5.9).

In the derivation of Eqs. (5.14a,b), there are terms of order $1/\gamma^2$ which have been neglected. From the expression for E_ϕ given in Eq. (5.2), it is seen that the coefficient of $\partial V_{1,k}/\partial \xi$ is of order $1/\gamma^2$, while that of $\partial V_{2,k}/\partial \xi$ is of order unity. Hence, the leading correction to E_ϕ arising due to the conducting plates is correctly determined from Eq. (5.14b). However, to determine the result to order $1/\gamma^2$, it is necessary to include the order $1/\gamma^2$ correction to Eq. (5.14b).

To proceed, we must improve the previous treatment of the retardation condition of Eq. (5.5) by using the approximation $\beta \approx 1 - 1/2\gamma^2$ rather than $\beta \approx 1$. In this case, Eq. (5.9) is replaced by

$$\frac{x}{k^{3/2}} = \frac{y_k^4 - 3}{6y_k} + \frac{1}{2\gamma^2} \frac{y_k}{k\Delta}. \tag{5.15}$$

Also, we must employ $\beta \approx 1 - 1/2\gamma^2$ in Eq. (5.3b), obtaining

$$V_{2,k} \approx \frac{2}{(k\Delta)^{1/2}} \left[\frac{y_k^3}{1+y_k^4} - \frac{y_k^5}{(1+y_k^4)^2} \frac{1}{k\Delta\gamma^2} \right]. \tag{5.16}$$

Then, using Eq. (5.13a) to determine $\partial V_{2,k}/\partial \xi$, with $\partial y/\partial x$ computed

from Eq. (5.15), we find

$$\frac{\partial V_{2,k}}{\partial \xi} \approx \frac{4}{(k\Delta)^2}\left[\frac{y_k^4(3-y_k^4)}{(1+y_k^4)^3} - \frac{1}{k\Delta\gamma^2}\frac{y_k^6(8-4y_k^4)}{(1+y_k^4)^4}\right]. \tag{5.17}$$

Let us now define Y_k by

$$\frac{x}{k^{3/2}} = \frac{Y_k^4 - 3}{6Y_k}. \tag{5.18}$$

From Eq. (5.15) it follows that

$$\frac{y_k^4 - 3}{6y_k} = \frac{Y_k^4 - 3}{6Y_k} - \frac{y_k}{2k\Delta\gamma^2}. \tag{5.19}$$

We see that $Y_k = y_k$ if order $1/\gamma^2$ terms are neglected, and

$$y_k - Y_k \approx -\frac{Y_k^3}{k\Delta\gamma^2(1+Y_k^4)}. \tag{5.20}$$

The tangential electric field on the orbit can be determined from Eq. (5.2), with $\partial V_{1,k}/\partial\xi$ and $\partial V_{2,k}/\partial\xi$, $k \neq 0$, given, respectively, by Eqs. (5.14a) and (5.17). The $k=0$ fields are as presented in Eqs. (3.10) and (3.11). In this manner we obtain for $|\xi| \lesssim \Delta \ll 1$, $\gamma^2\Delta \gg 1$:

$$\begin{aligned} E_\phi \cong \frac{e}{4\rho^2\gamma^2}&\left[\frac{\cos\xi}{\sin^2\xi} + \frac{1}{\Delta^3}G_1(\xi/\Delta^{3/2})\right] \\ &- \frac{4}{3}\frac{e\gamma^4}{\rho^2}\left[w(3\gamma^3\xi) - \frac{3}{8}\frac{1}{\Delta^2\gamma^4}G_2(\xi/\Delta^{3/2})\right], \end{aligned} \tag{5.21}$$

where

$$G_1(\xi/\Delta^{3/2}) = 2\sum_{k=1}^{\infty}\frac{(-1)^{k+1}}{k^3}\left[\frac{4Y_k^2(1-3Y_k^4)}{(1+Y_k^4)^3} - \frac{32Y_k^6(5-7Y_k^4)}{(1+Y_k^4)^5}\right] \tag{5.22a}$$

and

$$G_2(\xi/\Delta^{3/2}) = 2\sum_{k=1}^{\infty} \frac{(-1)^{k+1}}{k^2}\left[\frac{4Y_k^4(3 - Y_k^4)}{(1 + Y_k^4)^3}\right]. \tag{5.22b}$$

Equation (5.20) has been used to change variables from y_k to Y_k. It is clear from Eq. (5.18) that Y_k is a function only of the variable $\xi/(k\Delta)^{3/2}$, which shows that G_1 and G_2 are functions only of the scaled variable $\xi/\Delta^{3/2}$. The scaling functions G_1, G_2 are plotted in Figure 3.

Numerical calculations of the wakefield using the exact expression of Eqs. (5.2) and (5.3) are discussed in Appendix C. It is found that when $|\xi| \lesssim \Delta \ll 1$, the sum over k converges rapidly, and the scaling relation of Eq. (5.21) is verified. On the other hand, when $|\xi| \gg \Delta$, the convergence of the sum over k is found to be slow, and violation of the scaling behavior is to be expected, even for small Δ. One should note that the magnitude of the wakefield is very small when $|\xi| \gg \Delta$; therefore, from the point of view of estimating instabilities, only the interval $|\xi| \lesssim \Delta$ is important.

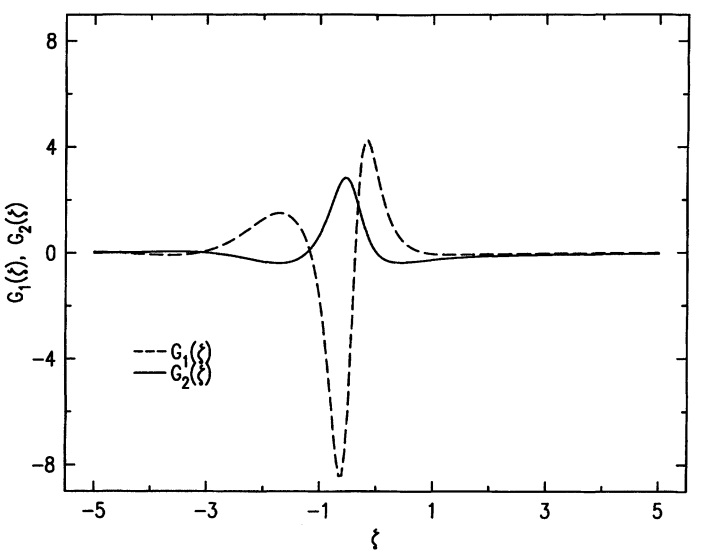

FIGURE 3 Plot of the parallel plate wakefield scaling functions $G_1(\zeta)$ and $G_2(\zeta)$ as given in Eqs. (5.22a,b).

In Section 5.2, we present an asymptotic analysis indicating that the exact wakefield decays as $\exp(-\pi|\xi|/\Delta)$ for $|\xi| \gg \Delta$. This form violates the scaling of Eq. (5.21). A non-leading term is also found which decays as $\exp[-(9/32)^{1/3}(\pi\xi^{2/3}/\Delta)]$, consistent with scaling. These results indicate the nature of the violation of scaling when $|\xi| \gg \Delta$.

In free space the radiation travels along a chord to another point on the circle, thereby always arriving before (in front) of the exciting charge. With the plates in place the radiation can bounce off the plates once or numerous times and arrive behind the exciting charge resulting in a trailing wakefield, which we have described using image charges. For $\gamma^2\Delta \gg 1$, the G_1 term is smaller than the G_2 term and for small ξ they are both small compared to the free space radiation wakefield, $w(3\gamma^3\xi)$. When $\gamma^2\Delta \approx 1$, the G_1, G_2 and w terms become comparable in magnitude, and the situation is more complicated.

5.2. Behavior of Wakefield for Large Separation

In free space, the wakefield has an algebraic fall off ($\sim \xi^{-4/3}$) for large distances (times). In the presence of the conducting plates, this algebraic fall off is cancelled by the fields due to the image charges, resulting in an exponential decay of the wakefield. This is the time-domain analog of the suppression of low frequencies in the resistive impedance due to the parallel plates. Here, we present a non-rigorous argument indicating the leading exponential behavior of the wakefield at large separations between the observation point and the source. In Eq. (5.2), we convert the sum over k into a contour integral in the complex k-plane. The contribution from $V_{2,k}$ involves the integral

$$\int_{C_1+C_2} \frac{\mathrm{d}k}{\sin \pi k} \frac{\sin^2 \alpha_k}{s_k - \sin \alpha_k \cos \alpha_k}, \tag{5.23}$$

where the contour $C_1 + C_2$ is illustrated in Figure 4. The quantity s_k was defined in Eq. (5.4).

The integration contour will be deformed, and the asymptotic behavior in ξ will be determined by the contribution of the singularities in the complex k-plane. One set of singularities is associated

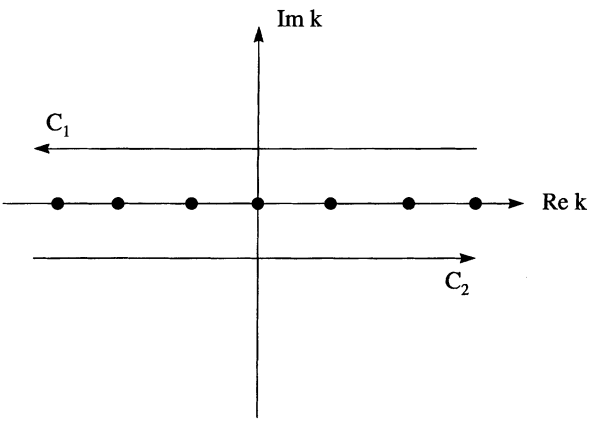

FIGURE 4 Sketch of the contour in the complex k-plane used to evaluate Eq. (5.23).

with the vanishing of the denominator when

$$\sqrt{\sin^2 \alpha_k + k^2\Delta^2} - \sin \alpha_k \cos \alpha_k = 0. \tag{5.24}$$

This condition provides a relationship between α_k and k,

$$\sin^4 \alpha_k = -k^2\Delta^2. \tag{5.25}$$

Now to solve for the singular value of k, we use the retardation condition

$$\begin{aligned} \xi &= \alpha_k - \sqrt{\sin^2 \alpha_k + k^2\Delta^2} \\ &= \alpha_k - \sin \alpha_k \cos \alpha_k. \end{aligned} \tag{5.26}$$

For small α_k, we find

$$\alpha_k \approx \left(\frac{3\xi}{2}\right)^{1/3} (1, e^{\pm 2i\pi/3}) \tag{5.27a}$$

and

$$k\Delta \approx \left(\frac{3\xi}{2}\right)^{2/3} (\pm i)(1, e^{\pm 4i\pi/3}). \tag{5.27b}$$

The absolute value of the contour integral is controlled by the limit

$$\frac{1}{\sin \pi k} \to e^{-(\pi/\Delta)|\mathrm{Im}(k\Delta)|}. \tag{5.28}$$

The smallest value of $|\mathrm{Im}(k\Delta)|$ is given by $(3\xi/2)^{2/3}\sin(\pi/6)$; hence the exponential decay is dominated by

$$\exp\left[-\frac{\pi}{\Delta}\left(\frac{9}{32}\right)^{1/3}\xi^{2/3}\right]. \tag{5.29}$$

Further consideration shows that the singularities are branch points in the complex k-plane, and not simple poles.

Another singularity arises from the branch point at $s_k = 0$, i.e.

$$\sin \alpha_k = \pm ik\Delta. \tag{5.30}$$

Using the retardation condition, which in this case is simply

$$\alpha_k = \xi, \tag{5.31}$$

we determine the location of the branch points at

$$k\Delta = \pm i \sin \xi \approx \pm i\xi. \tag{5.32}$$

The asymptotic behavior arises from the term

$$\frac{1}{\sin \pi k} \to e^{-\pi\xi/\Delta}. \tag{5.33}$$

Physically this exponential behavior corresponds to the evanescence of the electric field below cutoff in the parallel plate waveguide. We do not attempt to determine the functional dependence of the coefficients of the exponential factors of Eqs. (5.29) and (5.33).

This general result implies that the algebraic terms which can be extracted for large distances from G_1, G_2, w and the Coulomb term in Eq. (5.21) must all cancel. We have carried through the detailed calculation of all the $\xi^{-4/3}$ and ξ^{-2}/γ^2 terms and confirm their cancellation. In fact, the contribution to $V_{1,k}$ and $V_{2,k}$ cancel independently when one separates the w term into $V_{1,0}$ and $V_{2,0}$ parts at large distances.

In conclusion, our analysis suggests that the asymptotic behavior of the wakefield for large separations in front of the charge is given by

$$|E_\phi| \to \begin{cases} \xi^{-4/3}, & \dfrac{1}{3\gamma^3} \ll \xi \ll \dfrac{\Delta}{\pi}, \quad (5.34a) \\ \exp\left(-\dfrac{\pi\xi}{\Delta}\right), & \dfrac{\Delta}{\pi} \ll \xi \ll 1. \quad (5.34b) \end{cases}$$

In the regime of Eq. (5.34b), our analysis indicates the existence of terms with the non-leading behavior $\exp[-(9/32)^{1/3}(\pi\xi^{2/3}/\Delta)]$. The asymptotic behavior of the electric field behind the charge is given by Eq. (5.34b) with ξ replaced by $\psi = \pi - \xi$.

5.3. Wakefield at the Position of the Point Charge

To calculate the tangential electric field at the position of the electron itself ($\xi = 0$), we must keep terms of higher order in Δ when considering the contribution from $V_{2,k}$. From the retardation condition of Eq. (5.5), it follows that

$$\frac{d\alpha_k}{d\xi} = \frac{1}{1 - (\beta \sin 2\alpha_k)/(2s_k)}. \quad (5.35)$$

Hence from Eqs. (5.3) one can derive

$$\frac{\partial V_{1,k}}{\partial \xi} = \frac{\beta \cos 2\alpha_k - (\sin 2\alpha_k)/(2s_k)}{s_k^2[1 - (\beta \sin 2\alpha_k)/(2s_k)]^3}, \quad (5.36a)$$

$$\frac{\partial V_{2,k}}{\partial \xi} = \frac{(s_k - (\beta/2)\sin 2\alpha_k)\sin 2\alpha_k + \sin^2 \alpha_k(\beta \cos 2\alpha_k - (\sin 2\alpha_k)/(2s_k))}{s_k^2[1 - (\beta \sin 2\alpha_k)/(2s_k)]^3}. \quad (5.36b)$$

For $\xi = 0$, $\beta \sim 1$ and $\gamma^2\Delta \gg 1$, the retardation conditon of Eq. (5.5) becomes ($k \neq 0$)

$$\alpha_k = s_k. \quad (5.37)$$

When $k\Delta \ll 1$, the solution of Eq. (5.37) is approximately given by ($k \neq 0$)

$$\alpha_{k0} = (\sqrt{3}k\Delta)^{1/2}. \quad (5.38)$$

Using small-angle approximations for the trigonometric functions in Eq. (5.36b) we obtain

$$\left(\frac{\partial V_{2,k}}{\partial \xi}\right)_{\xi=0} = -\frac{3}{5}\frac{1}{\alpha_{k_0}^2}. \tag{5.39}$$

It follows from Eq. (5.2) that for $1/\gamma \ll \Delta \ll 1$:

$$E_\phi(0) = -\frac{2}{3}\frac{e}{\rho^2}\left[\gamma^4 + \frac{3\sqrt{3}\kappa_2}{10}\frac{1}{\Delta} + 0\left(\frac{1}{\gamma^2\Delta^3}\right)\right], \tag{5.40}$$

where

$$\kappa_2 \cong \sum_{k=1}^{\infty} \frac{(-1)^{k+1}}{k} = \ln 2. \tag{5.41}$$

In Eq. (5.40), we have averaged the singular free space contribution to the electric field immediately in front and behind the point charge. The second term cannot be obtained from Eq. (5.21) because $G_2(0) = 0$. It was necessary to go to higher order in Δ. The correction due to the conducting plates is small in magnitude, and has the sign indicating that the electron radiates more energy between the conducting plates than it would in free space. This is the case despite the fact that the plates cut off the lowest frequencies.

6. FREE SPACE IMPEDANCE

Until this point we have been considering the wakefield in the time domain. Now we consider its Fourier transform, the impedance. Introducing the azimuthal angle

$$\theta = 2\pi - 2\psi, \tag{6.1}$$

we define

$$E_{\phi,n} = \int_0^{2\pi} \frac{d\theta}{2\pi} e^{-in\theta} E_\phi(\theta), \tag{6.2}$$

and the impedance Z_n by

$$2\pi\rho E_{\phi,n} = -Z_n I_n, \tag{6.3}$$

where I_n is the Fourier coefficient of the electron current. For a single electron

$$I_n = \frac{ec\beta}{2\pi\rho}, \tag{6.4}$$

$$I(\theta) = \sum_{n=-\infty}^{\infty} I_n e^{in\theta}. \tag{6.5}$$

The real (radiated) power P_n and the reactive power Q_n are determined by

$$P_n + iQ_n = -ec\beta E_{\phi,n}. \tag{6.6}$$

From Eq. (6.3), it follows that

$$P_n = I_n^2(\mathrm{Re}\, Z_n), \tag{6.6a}$$

$$Q_n = I_n^2(\mathrm{Im}\, Z_n). \tag{6.6b}$$

When discussing synchrotron radiation, one usually considers the power $\wp_n$ radiated into the modes n and $-n$,

$$\wp_n = P_n + P_{-n} = 2P_n. \tag{6.7}$$

From Eq. (2.16), we take E_ϕ to be the non-singular field due to synchrotron radiation, dropping the singular Coulomb term. Converting to MKS units, we can write

$$E_\phi = \frac{-e}{4\pi\epsilon_0\rho^2} \sum_{m=1}^{\infty} (-1)^m f_m \cos m\left(\pi - \frac{\theta}{2}\right), \tag{6.8}$$

where

$$f_m = m\beta^2 J_m'(m\beta) - \frac{1}{2}(1-\beta^2)m^2 \int_0^\beta J_m(mx)\, dx. \tag{6.9}$$

The impedance is found to be given by ($Z_0 = 1/\epsilon_0 c$)

$$\frac{\beta}{\pi}\frac{Z_n}{Z_0} = \frac{1}{2} f_{2n} + \frac{i}{2\pi} \sum_{\substack{m=1 \\ (\text{odd})}}^{\infty} f_m \frac{2n}{(m/2)^2 - n^2}. \tag{6.10}$$

The Weber function $E_n(z)$ is defined[19] by

$$J_n(z) + iE_n(z) = \frac{1}{\pi} \int_0^{\pi} \mathrm{d}\theta \, \mathrm{e}^{i(n\theta - z\sin\theta)}, \tag{6.11}$$

and it can be expressed in a Kapteyn series[19]

$$E_{2n}(2n\beta) = \frac{2}{\pi} \sum_{\substack{m=1 \\ (\text{odd})}}^{\infty} J_m(m\beta) \frac{4n}{(2n)^2 - m^2}. \tag{6.12}$$

Using Eq. (6.12), we can express Eq. (6.10) in the form

$$\begin{aligned} \frac{\beta}{\pi}\frac{Z_n}{Z_0} &= n\beta^2 \left[J'_{2n}(2n\beta) - iE'_{2n}(2n\beta)\right] \\ &\quad - (1-\beta^2)n^2 \int_0^{\beta} \left[J_{2n}(2nx) - iE_{2n}(2nx)\right] \mathrm{d}x \\ &\quad - i(1-\beta^2)\frac{2n}{\pi} \sum_{\substack{m=1 \\ (\text{odd})}}^{\infty} \int_0^{\beta} J_m(mx)\, \mathrm{d}x. \end{aligned} \tag{6.13}$$

Employing the Kapteyn series[19]

$$\sum_{k=1}^{\infty} J_k(kx) = \frac{x}{2(1-x)}, \tag{6.14a}$$

$$\sum_{k=1}^{\infty} J_{2k}(2kx) = \frac{x^2}{2(1-x^2)}, \tag{6.14b}$$

the last term in Eq. (6.13) can be evaluated and we obtain

$$\frac{Z_n}{Z_0} = \pi n\beta\left[J'_{2n}(2n\beta) - iE'_{2n}(2n\beta)\right]$$
$$- \pi n^2\left(\frac{1-\beta^2}{\beta}\right)\int_0^\beta \left[J_{2n}(2nx) - iE_{2n}(2nx)\right]\mathrm{d}x$$
$$- i2n\left(\frac{1-\beta^2}{\beta}\right)\left(-\frac{1}{4}\right)\ln(1-\beta^2). \tag{6.15}$$

A similar but not totally equivalent expression for Z_n was given in Ref. 10.

If we consider the ultrarelativistic limit, $\beta \sim 1$, and restrict our attention to the region

$$1 \ll n \ll n_c, \tag{6.16}$$

where $n_c = 3\gamma^3/2$, then we can use

$$J'_{2n}(2n) \sim \frac{3^{1/6}\Gamma\left(\frac{2}{3}\right)n^{-2/3}}{2\pi}, \tag{6.17a}$$

$$E'_{2n}(2n) \sim \frac{-\Gamma\left(\frac{2}{3}\right)n^{-2/3}}{2\pi 3^{1/3}} \tag{6.17b}$$

and we find

$$Z_n \sim Z_0 n\pi\left[J'_{2n}(2n) - iE'_{2n}(2n)\right]$$
$$\sim \frac{Z_0\Gamma\left(\frac{2}{3}\right)}{3^{1/3}}\left(\frac{\sqrt{3}}{2} + \frac{i}{2}\right)n^{1/3}. \tag{6.18}$$

The asymptotic expression of Eq. (6.18) was discussed by Faltens and Laslett.[11] In this asymptotic form, the positive sign of the imaginary part corresponds to the fact that the wake function is large in front of the electron and negligible behind.

For $n \gg n_c$, one can evaluate the $\mathrm{Im}\, Z_n$ from Eq. (6.15) by using the limiting form for $E_{2n}(2nx)$, which can be derived from the integral

representation in Eq. (6.11). The result is

$$\operatorname{Im} Z_n \approx \frac{-2Z_0\gamma^4}{3}\frac{1}{n}, \tag{6.19}$$

which is consistent with the small μ limit of the wakefield given in Eq. (3.16).

For $1 \ll n \ll n_c$, only the J'_{2n} and E'_{2n} terms in Eq. (6.15) for the impedance are significant. These arise from the far field radiation. When $n \gg n_c$, all terms in the expression for the impedance are significant. This is because at very high frequencies, characteristic of very short distances, the near field also contributes to the impedance. The asymptotic form for the impedance when $n \gg n_c$ is

$$Z_n \approx Z_0\left[\frac{\sqrt{3}}{4}\left(\frac{\pi}{2}\right)^{1/2}\left(\frac{2n_c}{3}\right)^{1/3}\left(\frac{n}{n_c}\right)^{1/2} e^{-n/n_c} - i\left(\frac{2}{3}\right)^{7/3}\frac{n_c^{4/3}}{n}\right]. \tag{6.20}$$

Note that the real part of the impedance decays exponentially with increasing n while the imaginary part decays more slowly as the inverse of n. Using the results of Appendix A, we plot $\operatorname{Re} Z_n$ and $\operatorname{Im} Z_n$ as functions of n/n_c in Figure 5.

Physical insight into the connection between the time-domain wakefield and the frequency-domain coupling impedance can be had by noting that the two are a Fourier transform pair. For this characterization we need only consider the real part of the impedance. If one approximates $\operatorname{Re} Z_n$ as a step function extending from zero to n_c, the Fourier transform will have a width on the order of $(1/n_c)$ which is exactly the behavior of the short time wakefield. If one includes the fact that the impedance is not a constant step but grows as $\operatorname{Re} Z_n \propto n^{1/3}$ this yields the $\xi^{-4/3}$ asymptotic tail of the wakefield for large $\xi \gg 1/n_c$.

7. LONGITUDINAL COUPLING IMPEDANCE WITH PARALLEL PLATES

The longitudinal coupling impedance of a charge circulating on an orbit of radius ρ in the midplane between two conducting plates has

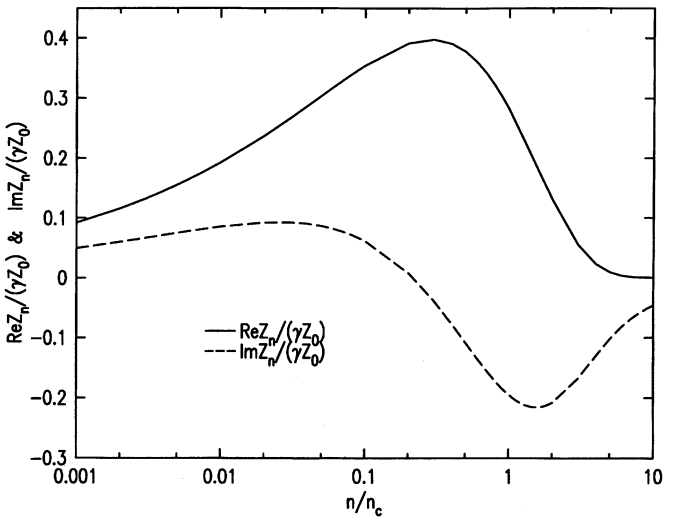

FIGURE 5 Plot of the free space impedance $\mathrm{Re}\,Z_n$ and $\mathrm{Im}\,Z_n$ versus n for an extensive range of n including $n > n_c$.

been derived by several authors:[3,5,7,11,13–16]

$$Z_{\mathrm{pp}}(n) = \frac{2\pi^2 n Z_0}{\beta}\frac{\rho}{2h}\sum_{p\,(\mathrm{odd})\geq 1}\Lambda_p \cdot \{\beta^2 J_n'(\gamma_p\rho)[J_n'(\gamma_p\rho) + iY_n'(\gamma_p\rho)] + (\alpha_p/\gamma_p)^2 J_n(\gamma_p\rho)[J_n(\gamma_p\rho) + iY_n(\gamma_p\rho)]\}, \tag{7.1}$$

where

$$\alpha_p^2 = \left(\frac{p\pi}{2h}\right)^2, \qquad \gamma_p^2 = \frac{n^2\beta^2}{\rho^2} - \alpha_p^2,$$

h is the distance of each of the plates from the electron beam,

$$\Lambda_p = \sin\left(\frac{p\pi\,\delta h}{2h}\right)\Big/\left(\frac{p\pi\,\delta h}{2h}\right)$$

and δh is the vertical thickness of the electron beam. When considering the real part of the impedance Λ_p can be set to unity. However, when considering the imaginary part of impedance Λ_p must be used in the above form to properly introduce a cutoff for the divergence due to the Coulomb field.

The real part of this impedance is given by

$$\operatorname{Re} Z_{\mathrm{pp}}(n) = \frac{2\pi^2 n Z_0}{\beta} \frac{\rho}{2h} \sum_{p(\mathrm{odd}) \geq 1}^{n\beta 2h/\pi\rho} \left\{ \beta^2 J_n'^2(\gamma_p \rho) + \left(\frac{\alpha_p}{\gamma_p}\right)^2 J_n^2(\gamma_p \rho) \right\}, \tag{7.2}$$

and is non-zero only for $n \geq \pi\rho/(2h\beta)$, which is characteristic of the simple waveguide cutoff of the parallel plate resonator. In this form the first term corresponds to the emission of radiation which is polarized in the plane of the electron orbit and the second term corresponds to radiation which is polarized perpendicular to the midplane.

The real part of the impedance can also be written as

$$\operatorname{Re} Z_{\mathrm{pp}}(n) = 2\pi^2 \beta n Z_0 \frac{\rho}{2h} \sum_{1 \leq p(\mathrm{odd})}^{n2h\beta/\rho\pi} \left[J_n'^2(n\beta \cos\theta_p) + \frac{\tan^2\theta_p}{\beta^2} J_n^2(n\beta \cos\theta_p) \right], \tag{7.3}$$

where

$$\alpha_p^2 = \left(\frac{p\pi}{2h}\right)^2 = \frac{\omega^2}{c^2} \sin^2\theta_p, \qquad \gamma_p^2 = \frac{\omega^2}{c^2} - \alpha_p^2 = \frac{\omega^2}{c^2} \cos^2\theta_p$$

and the definition of θ_p is given by

$$\sin\theta_p = \frac{p\pi c}{2h\omega} = \frac{p\pi\rho}{2hn\beta}. \tag{7.4}$$

The summation over p adds the contributions of radiation from emission at different vertical angles. Note that in the parallel plate case the transverse wave number, $p\pi/(2h)$, is quantized and therefore the angles of emission are also quantized. In the limit of $h \to \infty$ the sum over p can be converted to an integral over all vertical angles and it can be shown in a straightforward manner that this real part of the parallel plate impedance goes over to the real part of the free space impedance as required.

If we consider $\beta \approx 1$ and large n, then

$$\sin\theta_p = \frac{\pi p}{2\Delta n} = \frac{n_p}{n} \approx \theta_p, \tag{7.5}$$

with $\Delta = h/\rho$.

Near $\theta_p = 0$, the Bessel functions in Eq. (7.3) can be written in terms of the modified Bessel functions $K_{1/3}$ and $K_{2/3}$. Defining

$$x \approx n\left[1 - \frac{1}{2\gamma^2} - \frac{\theta^2}{2}\right],$$

we can write for $n \gg 1$

$$J_n(x) \approx \frac{1}{\sqrt{3}\pi}\left(\frac{1}{\gamma^2} + \theta^2\right)^{1/2} K_{1/3}\left[\frac{n}{3}\left(\frac{1}{\gamma^2} + \theta^2\right)^{3/2}\right], \tag{7.6a}$$

$$J_n'(x) \approx \frac{1}{\sqrt{3}\pi}\left(\frac{1}{\gamma^2} + \theta^2\right) K_{2/3}\left[\frac{n}{3}\left(\frac{1}{\gamma^2} + \theta^2\right)^{3/2}\right]. \tag{7.6b}$$

We make use of the following approximations:

$$\frac{n}{3}\left(\frac{1}{\gamma^2} + \theta_p^2\right)^{3/2} \approx \frac{n_p^3}{3n^2} \quad \text{for } n \ll n_c = \frac{3}{2}\gamma^3, \tag{7.7a}$$

$$K_n(y) \approx \sqrt{\frac{\pi}{2y}}\,e^{-y} \quad \text{for large } y = \frac{n_p^3}{3n^2}. \tag{7.7b}$$

Using the above approximations, the first term in Eq. (7.3) can be rewritten for $1 \le n \le n_p^{3/2}$ as

$$\begin{aligned} \operatorname{Re} Z_{\mathrm{pp}}(n)\big|_p &\propto n \cdot n_1 \cdot J_n'^2(n\beta\cos\theta_p) \\ &\propto n \cdot n_1 \cdot \theta_p^4 \cdot K_{2/3}^2\left[\frac{n_p^3}{3n^2}\right] \propto \frac{n_1 n_p}{n}\exp\left[-\frac{2n_p^3}{3n^2}\right]. \end{aligned} \tag{7.8}$$

Using $\tan^2\theta_p \approx \theta_p^2$, the other term simply doubles the contribution as the large argument approximation for K_n does not depend on n. Including all the constant factors, we find

$$\operatorname{Re} Z_{\mathrm{pp}}(n) \approx \sum_{p(\mathrm{odd})=1}^{\infty} 2Z_0 \frac{n_1 n_p}{n}\exp\left[-\frac{2n_p^3}{3n^2}\right], \tag{7.9}$$

where the replacement of the K-Bessel functions by the exponential asymptotic form in the pth term is justified only when $1 \ll n \ll n_p^{3/2}$, which would limit the applicability of the full sum to $n \ll n_1$. However, the sum still provides a useful approximation to $\mathrm{Re}\, Z_{\mathrm{pp}}$ for all $n_1 \ll n \ll n_c$ because when the exponential approximation to the K-Bessel function is less accurate the contribution to the sum is small. In fact, if the sum over p in Eq. (7.9) is converted to an integral, the integration can be done analytically resulting in the expression

$$\mathrm{Re}\, Z_n \approx \left(\frac{2}{3}\right)^{1/3} \frac{Z_0 \Gamma\left(\frac{2}{3}\right)}{2} n^{1/3}, \tag{7.10}$$

which differs from the exact asymptotic expression Eq. (6.18) by only a factor of $(2/3)^{1/3}/3^{1/6}$.

For $p=1$, Eq. (7.9) is precisely Warnock's[15] approximate expression. Note that $\mathrm{Re}\, Z_{\mathrm{pp}}(n)$ remains vanishingly small for values of n in excess of the simple waveguide cutoff. As such, it has been suggested that the "cutoff" should be given by

$$n_{\mathrm{co}} = \sqrt{\frac{2}{3}} n_1^{3/2} = \sqrt{\frac{2}{3}} \left(\frac{\pi}{2\Delta}\right)^{3/2}. \tag{7.11}$$

Recall that the wakefield in the parallel plate geometry [Eq. (5.21)] exhibited the corresponding scaling in the variable $\xi \Delta^{-3/2}$.

We can give an intuitive argument yielding insight into Eq. (7.11). One can think of the pth waveguide mode as bouncing between the parallel plates at an angle θ_p [Eq. (7.4)] relative to the midplane. The cutoff frequency corresponds to $\sin\theta_p = n_p/n = 1$, i.e. $n = n_p = p\pi/2\Delta$. The vertical angular distribution of synchrotron radiation at frequency $\omega = nc/\rho$ is characterized by the emission angle[18]

$$\theta_{\mathrm{rad}} = \left(\frac{3}{2n}\right)^{1/3} \quad (n \ll n_c). \tag{7.12}$$

The emission of the pth mode will be suppressed for

$$\theta_p \gg \theta_{\mathrm{rad}}, \tag{7.13}$$

that is for

$$n \ll \sqrt{\frac{2}{3}} n_p^{3/2}, \tag{7.14}$$

as is exhibited in Eq. (7.9).

In Figure 6 we plot $\mathrm{Re}\, Z_{\mathrm{pp}}(n)$ versus n ($n \ll n_c$) for several values of the parameter $\Delta = h/\rho$. Included in the figure for comparison is the free space asymptote,

$$\mathrm{Re}\, Z_n \approx Z_0 \cdot \frac{\Gamma(\frac{2}{3})}{3^{1/3}} \frac{\sqrt{3}}{2} n^{1/3}.$$

A good estimate of the local maximum value of $\mathrm{Re}\, Z_{\mathrm{pp}}$ can be computed from the impedance given in Eq. (7.9), $\mathrm{Re}\, Z_{\mathrm{pp}}^{\max}(n) \approx Z_0 \beta \sqrt{3} n_1^{1/2} \exp[-1/2]$ and it occurs at $\hat{n} = 2n_1^{3/2}/\sqrt{3}$. This peak value of $\mathrm{Re}\, Z_{\mathrm{pp}}$ (n) is 30% larger than the free space result. All of the curves for finite Δ have the same characteristic behavior. They start out from zero in the neighborhood of n_{co} and grow to a value roughly 30% larger than the free space value and then undershoot slightly before becoming equal to the free space value thereafter.

To emphasize the self-similarity of Z_{pp}, we plot $\Delta^{1/2}[\mathrm{Re}\, Z_{\mathrm{pp}} - \mathrm{Re}\, Z_{\mathrm{FS}}]/Z_0$ versus $n\Delta^{3/2}$ in Figure 7. It is seen that the several curves of Figure 6 merge to lie on a single curve in Figure 7. We also see the approach of Z_{pp} to Z_{FS} as n increases.

The imaginary part of the impedance contains two types of terms:

$$\begin{aligned}\mathrm{Im}\, Z_{\mathrm{pp}}(n) = \frac{2\pi^2 n Z_0}{\beta} \frac{\rho}{2h} \Bigg[& \sum_{\substack{p(\mathrm{odd}) \geq 1 \\ \gamma_p \text{ real}}}^{n\beta 2h/\pi\rho} \Bigg\{ \beta^2 J_n'(\gamma_p \rho)\, Y_n'(\gamma_p \rho) \\ & + \left(\frac{\alpha_p}{\gamma_p}\right)^2 J_n(\gamma_p \rho)\, Y_n(\gamma_p \rho) \Bigg\} + \sum_{\substack{p(\mathrm{odd}) \geq \\ n\beta 2h/\pi\rho \\ \mu_p \text{ real}}} \Lambda_p \frac{2}{\pi} \Bigg\{ \beta^2 I_n'(\mu_p \rho) K_n'(\mu_p \rho) \\ & + \left(\frac{\alpha_p}{\mu_p}\right)^2 I_n(\mu_p \rho) K_n(\mu_p \rho) \Bigg\} \Bigg],\end{aligned} \tag{7.15}$$

where $\mu_p = \sqrt{\alpha_p^2 - n^2\beta^2/\rho^2}$.

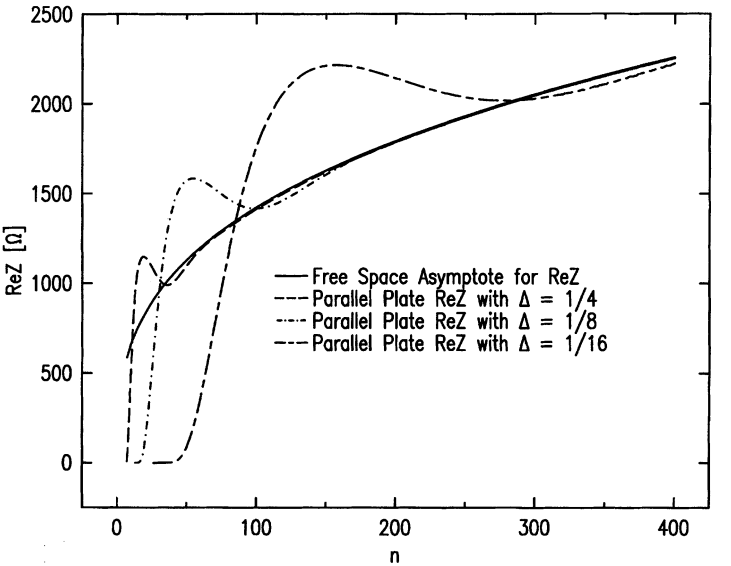

FIGURE 6 Plot of the parallel place impedance $\mathrm{Re}\, Z_{\mathrm{pp}}$ versus n ($n \ll n_c$) for several values of the parameter $\Delta = h/\rho$. Included in the figure for comparison is the real part of the free space impedance.

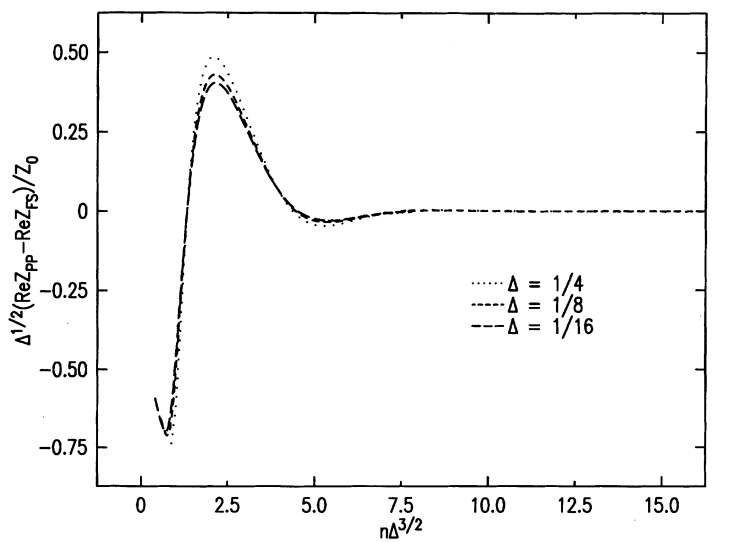

FIGURE 7 Plot of the same parallel plate data as in Figure 6 with the axes scaled to display the self-similarity of the real part of the impedance, $\mathrm{Re}\, Z_{\mathrm{pp}}$, for the values of the parameter $\Delta = h/\rho$ included in Figure 6.

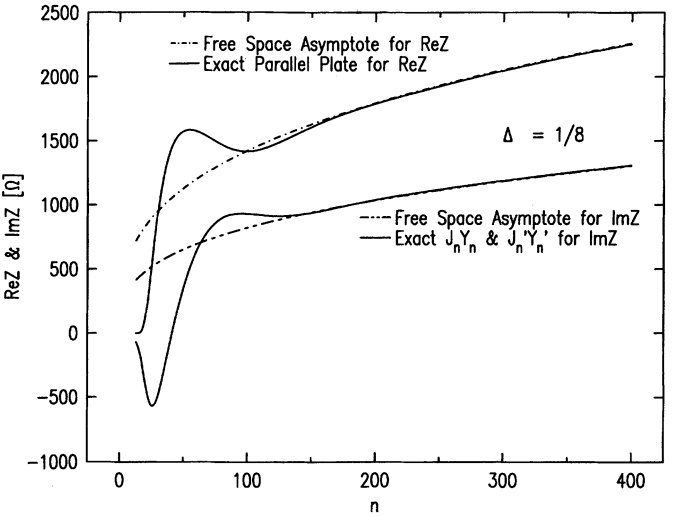

FIGURE 8 Plot of the real part of the parallel plate impedance, $\mathrm{Re}\, Z_{pp}$, and the JY and $J'Y'$ contributions to the imaginary part of the parallel place impedance for $\Delta = 1/8$. For comparison we also show the real and imaginary parts of the free space impedance.

The JY and $J'Y'$ terms in the above expression are the counterpart of the imaginary part of the radiation impedance in free space and as such the form factor Λ_p can be taken to be unity. The JY and $J'Y'$ terms of $\mathrm{Im}\, Z$ together with $\mathrm{Re}\, Z$ are plotted versus n in Figure 8. From Figure 8 it is seen that for sufficiently large n this contribution to $\mathrm{Im}\, Z_n$ is asymptotically equal to the reactive part of the free space radiation impedance, supporting the notion that at least for large n, these terms are the reactive part of the impedance arising from radiation in the presence of the parallel plates. Presumably, the IK and $I'K'$ terms (which are divergent in the absence of a high frequency cutoff) arise from the space charge effect in the presence of the parallel plates.

8. COHERENT RADIATED POWER

The total coherent power radiated by a current distribution is given by

$$P = 2\sum_{n=1}^{\infty} I_n^2 \,\mathrm{Re}\, Z(n). \tag{8.1}$$

8.1. Single Electron

For a single electron, I_n is a constant given by Eq. (6.4), and hence the power is simply determined by a sum over the real part of the impedance:

$$P = 2\left(\frac{ec\beta}{2\pi\rho}\right)^2 \sum_{n=1}^{\infty} \mathrm{Re}\, Z(n). \tag{8.2}$$

For an electron circulating in free space the real part of the impedance, $\mathrm{Re}\, Z(n)$, is given in Eq. (6.13). The seemingly complicated summation over Bessel functions can be done exactly to yield the following expression for the power radiated by a single charge in free space:[1]

$$P = \frac{2ce^2\beta^4\gamma^4}{3\rho^2}. \tag{8.3}$$

This is the same result obtained earlier in Section 3 when one takes $N=1$ in Eq. (3.18).

In the presence of infinitely conducting parallel plates, I_n is still given by Eq. (6.4), but now Eq. (7.2) must be used for $\mathrm{Re}\, Z(n)$. In this case there is no simple analytic expression for the power so one must resort to qualitative discussions and numerical techniques. From Figure 6 it can be seen that there are five distinct regions of interest when discussing the qualitative behavior of $\mathrm{Re}\, Z_{pp}(n)$. Starting from $n=0$, $\mathrm{Re}\, Z_{pp}(n)=0$ well below cutoff, then there is a region where $\mathrm{Re}\, Z_{pp}(n) < \mathrm{Re}\, Z_{FS}(n)$. This is followed by a region where $\mathrm{Re}\, Z_{pp}(n) > \mathrm{Re}\, Z_{FS}(n)$. In the fourth region $\mathrm{Re}\, Z_{pp}(n) < \mathrm{Re}\, Z_{FS}(n)$ again. Finally for $n \gg n_{co}$, $\mathrm{Re}\, Z_{pp}(n) = \mathrm{Re}\, Z_{FS}(n)$. This implies that the presence of the conducting plates suppresses the power radiated in regions 1, 2 and 4 of the spectrum, increases the power radiated in region 3, and in region 5 the radiated power is equal to the free space result. By computing the sum of the parallel plate impedance in the five regions numerically, one obtains the surprising result that slightly more power is radiated with the plates in place than in free space! A similar conclusion was obtained in Section 5 by considering the parallel plate wakefield to determine the power radiated by a single charge. In Eq. (5.40) it is seen that the small additional power scaled at Δ^{-1}. Note that this result has only been obtained for $n_{co} \ll n_c$, but

this is always true for realistic plate separations and relativistic electron beams.

8.2. Gaussian Electron Bunch

For the Gaussian electron bunch,

$$I_n = \frac{Nec\beta}{2\pi\rho} \exp\left[-\frac{1}{2}\left(\frac{n\sigma}{\rho}\right)^2\right]. \tag{8.4}$$

Due to the exponential decay of the I_n, the approximate expression for the free space impedance, Eq. (6.18), can be used to write the coherent power in CGS units as

$$P = \frac{3^{1/6}\Gamma(2/3)}{\pi} \frac{N^2e^2c}{\rho^2} \sum_{n=0}^{\infty} n^{1/3} \exp\left[-\frac{n^2\sigma^2}{\rho^2}\right], \tag{8.5}$$

where it has been assumed that the current decays fast enough that the upper limit on the sum can be taken to be infinity. If the above sum is approximated as an integral, the integral can be recognized to be a gamma function, so the coherent power radiated by a Gaussian electron bunch in free space can be written in CGS units as

$$P_{\mathrm{FS}} = \frac{N^2e^2c}{\rho^{2/3}\sigma^{4/3}} \frac{3^{1/6}\Gamma^2(2/3)}{2\pi}. \tag{8.6a}$$

This result is seen to agree with Schiff[3] upon taking his bunch width parameter $\phi = 2\sqrt{2}\sigma$. It is straightforward to rewrite Eq. (8.6a) in the form

$$P_{\mathrm{FS}} = \frac{N^2e^2c}{\rho^{2/3}\sigma^{4/3}} \frac{\Gamma(5/6)}{6^{1/3}\sqrt{\pi}}, \tag{8.6b}$$

in agreement with Eq. (3.28) derived using the wakefield. For computational purposes Eq. (8.6) is written in the more useful form as

$$P_{\mathrm{FS}}[\mathrm{W}] = 2.42 \times 10^{-20} \frac{N^2}{\rho^{2/3}[\mathrm{m}]\sigma^{4/3}[\mathrm{m}]}, \tag{8.7}$$

where P is in watts, and ρ and σ are in meters.

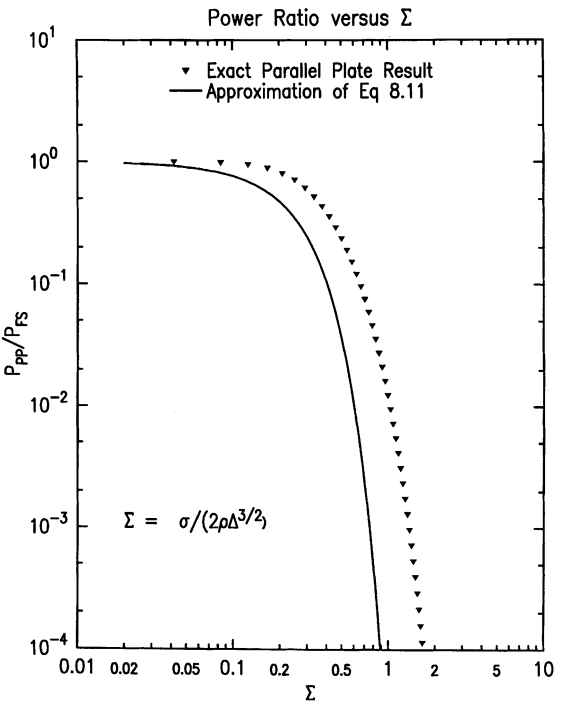

FIGURE 9 For a Gaussian bunch we plot the ratio of the coherent power radiated between parallel plates to that radiated in free space versus the scaling parameter Σ, defined in Eq. (8.8).

To accurately compute the coherent power radiated by a Gaussian electron beam in the presence of conducting plates one must resort to numerical analysis as the expressions are very complicated. In Figure 9 we plot the ratio of the coherent radiated power for the Gaussian electron bunch circulating between parallel plates to the coherent radiated power for the same bunch in free space, versus the scaling parameter, Σ, which is defined as

$$\Sigma \equiv \frac{\sigma}{2\rho\Delta^{3/2}}. \tag{8.8}$$

The parameter Σ compares the width σ/ρ of the current spectrum with the range of the wakefield $2\Delta^{3/2}$. To obtain the coherent radiated power for a Gaussian electron bunch circulating between parallel plates, first use Eq. (8.7) to compute the free space power, then

compute Σ and obtain the ratio P_{PP}/P_{FS} from Figure 9, then multiply the free space power by the ratio P_{pp}/P_{FS} to obtain the desired result. The data points in Figure 9 are an amalgam constructed from several values of $\Delta = 1/8$, $1/16$, $1/32$ and $1/64$ and numerous values of σ/ρ. It can be seen that for $\Sigma \ll 1$ the plates have little effect, and Eq. (8.7) alone can be used to estimate the radiated power.

In order to discuss some approximate expressions for the radiated power we follow Ref. 20. These authors introduce the parameter, x_{th}, which is related to Σ as follows:

$$x_{th} \equiv \frac{2}{3}\left(\frac{\pi}{2\Delta}\right)^3\left(\frac{\sigma}{\rho}\right)^2 = \frac{\pi^3}{3}\Sigma^2. \tag{8.9}$$

Ref. 19 suggests that the approximate impedance given in Eq. (6.18) can be used to give an approximation for the coherent power in CGS units,

$$P(x_{th}) \approx \frac{3^{1/6}N^2ce^2\Gamma(2/3)}{2\pi\rho^{2/3}\sigma^{4/3}}F(x_{th}), \tag{8.10}$$

where

$$F(x_{th}) \equiv \int_{x_{th}}^{x_c} \frac{e^{-x}}{x^{1/3}}dx \quad \text{and} \quad x_c \equiv \frac{9}{4}\left(\frac{\sigma}{\rho}\right)^2\gamma^6.$$

It can be shown that $x_c \to \infty$ does not introduce any significant error, and the integral in Eq. (8.10) reduces to the incomplete Γ-function of order 2/3. In this case the ratio of the power between the plates to the free space result is simply given as

$$\frac{P_{pp}}{P_{FS}} = \frac{F(x_{th})}{\Gamma(2/3)}. \tag{8.11}$$

To gauge the accuracy of this approximate expression, in Figure 9 we plot the ratio as given in Eq. (8.11) together with the more exact result discussed above. The approximation in terms of the incomplete gamma function is seen to consistently underestimate the coherent radiated power.

9. WAKEFIELD FOR A BUNCH OF ELECTRONS

In the previous sections we have derived expressions for the tangential electric field due to a single point electron. As in Eq. (3.10), let us denote by $\tilde{E}$ this electric field due to a point charge, with the singular space charge contribution removed. From Eq. (3.20) we recall that the coherent power loss P_c for a bunch of electrons is given by

$$P_c = -\beta ce \int_{-\infty}^{\infty} ds' \int_{-\infty}^{\infty} ds'' \tilde{E}_\phi(s' - s'')n(s')n(s''), \tag{9.1}$$

the sign is so chosen that P_c is positive for power loss by the electron beam. The beam profile is described by the number density $n(s)$, and we shall take this to be Gaussian,

$$n(s) = \frac{N}{\sqrt{2\pi}\sigma} e^{-s^2/2\sigma^2}, \tag{9.2}$$

We can define a wakefield for the bunch by

$$\tilde{W}(s) = -\int_{-\infty}^{\infty} ds' \tilde{E}_\phi(s - s')n(s'). \tag{9.3}$$

In Eqs. (9.1)–(9.3) we are using the arc length $s = 2\rho\xi$ as the variable specifying the location of the electrons, and since for highly relativistic particles the range of the wakefield is very small compared to the circumference of the orbit, we extend the range of integration to be from $-\infty$ to $+\infty$. The coherent power loss can be written in terms of the wakefield as

$$P_c = \beta ce \int_{-\infty}^{\infty} ds \tilde{W}(s)n(s). \tag{9.4}$$

9.1. Free Space

In free space, the non-singular part of the tangential electric field due to synchrotron radiation can be written as

$$\tilde{E}_\phi = -\frac{4}{3} \frac{e\gamma^4}{\rho^2} \frac{dv(\mu)}{d\mu}, \tag{9.5}$$

by using Eqs. (3.11) and (3.12). Employing Eq. (9.5) in Eq. (9.3), we carry out a partial integration to derive

$$\tilde{W}(x\sigma) = \frac{Ne}{(3\rho^2)^{1/3}} \frac{1}{\sigma^{4/3}} \sqrt{\frac{2}{\pi}} \frac{\partial}{\partial x} \int_0^\infty y^{-1/3} e^{-(1/2)(x-y)^2} \, dy, \tag{9.6}$$

where $v(\mu)$ has been replaced by its large argument approximation,

$$v(\mu) \approx \frac{9}{4 \cdot 3^{1/3}} \mu^{-1/3} \quad (\mu \gg 1). \tag{9.7}$$

Equation (9.6) can be used to express $\tilde{W}(s)$ in terms of the parabolic cylinder function $D_{1/3}(z)$, yielding[6,8]

$$\tilde{W}(s) = \sqrt{\frac{2}{\pi}} \frac{Ne}{(3\rho^2\sigma^4)^{1/3}} \Phi(s/\sigma), \tag{9.8}$$

with

$$\Phi(x) = \Gamma(2/3) e^{-x^2/4} D_{1/3}(-x). \tag{9.9}$$

The function $\Phi(x)$ is plotted in Figure 10.

9.2. Parallel Plates

In the presence of infinitely conducting parallel plates, the contribution of image charges must be added to the free space result. From Eq. (5.21), it is seen that the non-singular part of the electric field due to a point electron can be well approximated by the following expression when $1/\gamma^2 \ll \Delta \ll 1$:

$$\tilde{E}_\phi(s) = -\frac{4}{3} \frac{e\gamma^4}{\rho^2} \left[\frac{dv(\mu)}{d\mu} - \frac{3}{8} \frac{1}{\Delta^2\gamma^4} G_2\left(\frac{s}{2\rho\Delta^{3/2}}\right) \right]. \tag{9.10}$$

Now using Eqs. (9.8), (9.9) and (9.3), we derive

$$\tilde{W}(x\sigma) = \frac{Ne}{(3\rho^2\sigma^4)^{1/3}} \sqrt{\frac{2}{\pi}} \left[\Phi(x) - \left(\frac{3}{4}\right)^{1/3} \Sigma^{4/3} \int_{-\infty}^{\infty} dy \, G_2(\Sigma y) e^{-(1/2)(x-y)^2} \right], \tag{9.11}$$

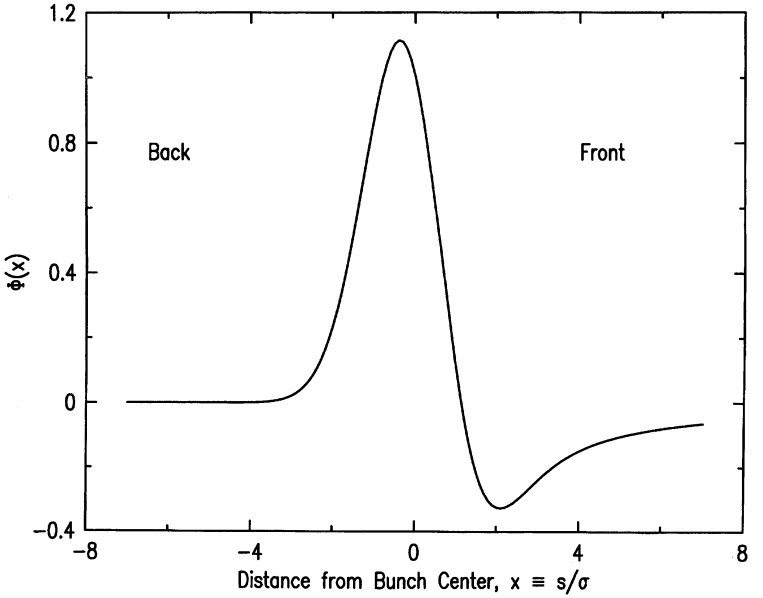

FIGURE 10 Plot of the function $\Phi(x)$ as given in Eq. (9.9), which determines the wakefield of a Gaussian bunch via Eq. (9.8).

where Σ was defined in Eq. (8.8) to be

$$\Sigma = \frac{\sigma}{2\rho\Delta^{3/2}} = \frac{\sigma}{2h}\left(\frac{\rho}{h}\right)^{1/2}. \tag{9.12}$$

In the case when $\Sigma \ll 1$,

$$\tilde{W}(x\sigma) \approx \frac{Ne}{(3\rho^2\sigma^4)^{1/3}}\sqrt{\frac{2}{\pi}}\left[\Phi(x) - \left(\frac{3}{4}\right)^{1/3}\sqrt{2\pi}\,\Sigma^{4/3}G_2(\Sigma x)\right]. \tag{9.13}$$

10. CONCLUDING REMARKS

There is a long history to the study of the electric field produced by an electron moving on a circular orbit. For the case of an electron moving in free space, an expression for the tangential electric field on the circular orbit was given back in 1912 by Schott,[1] in his treatise

on electromagnetics. For a relativistic electron we have been able to simplify Schott's results, and we have derived a useful expression for the short-range wakefield. The longitudinal impedance has been determined via Fourier transform.

For an electron moving on a circular orbit between parallel plates, the electric field was determined by Nodvick and Saxon.[3] Whereas Schott's free space results were obtained by working in the time-domain, the results of Nodvick and Saxon were found by working in the frequency domain. In our paper, we have solved the parallel plate problem by working in the time domain, utilizing the method of image charges. As is often the case, time and frequency domain results are complementary, each illuminating different aspects of the problem.

The free space wakefield can be separated into a "Coulomb term" and a "radiation term." The Coulomb term, which exists in equal magnitude both in front and in back of the exciting charge, is simply the manifestation of the static Coulomb field which is carried along by the electron but is corrected for the relativistic motion of the electron, $E \propto 1/\gamma^2 s^2$. The radiation wakefield has the peculiar characteristic that it is predominantly in front of the exciting charge; this is due to the presence of the factor $(1 + \beta \cos \chi)$ in the denominator of the expression for the radiation wakefield. The free space radiation wakefield has a single scale factor, $\mu = \frac{3}{2}\gamma^3 s/\rho$. The radiation wakefield is such that charges within a distance, $0 < \mu < 2.7$, of the exciting charge lose energy while charges further away ($\mu > 2.7$) gain energy from the exciting charge. For $\mu \gg 2.7$, the radiation wakefield is given by

$$\tilde{E}_\phi(s) \approx \frac{2e}{3^{4/3}\rho^{2/3}s^{4/3}},$$

which is independent of the energy of the exciting charge and decays slower with distance than the Coulomb term.

If infinitely conducting plates are introduced on the top and bottom of the circulating charge, the wakefield can be found using the method of images. In this case an additional scale factor appears, $\Delta^{3/2} = (h/\rho)^{3/2}$, which is characteristic of the separation $2h$ of the plates. For small distances $s \ll \rho\Delta^{3/2}$ in front of the exciting charge,

the wakefield remains essentially unchanged from the free space wakefield. However, for large distances, $s \gg \rho\Delta^{3/2}$, the wakefield now decays exponentially with distance far from the exciting charge.

The longitudinal coupling impedance is the frequency domain counterpart of the radiation wakefield. In free space, both $\mathrm{Re}\, Z$ and $\mathrm{Im}\, Z$ grow with frequency as $n^{1/3}$ in the range $0 < n < n_c$. This behavior arises since $n^{1/3}$ is the Fourier transform of the long tail of the wakefield $\tilde{E}_\phi(s) \propto s^{-4/3}$. Beyond n_c, $\mathrm{Re}\, Z$ decays exponentially with n while $\mathrm{Im}\, Z$ decays much slower as $1/n$. The power spectrum of synchrotron radiation is given by $\mathrm{Re}\, Z$.

In the parallel plate case, the low frequency part of the impedance, for $n \ll \Delta^{-3/2}$, is suppressed while the high frequency part of the impedance, for $n \gg \Delta^{-3/2}$, remains unchanged from the free space result. In the connecting region, $n \approx \Delta^{-3/2}$, the real part of the parallel plate impedance actually exceeds the free space impedance and its peak value is proportional to $\Delta^{-1/2}$.

An intense source of coherent synchrotron radiation could be provided by short bunches circulating in a storage ring. Suppose the circumference of the ring is $2\pi R$ and the dipole bending radius is ρ. If the bunch is short enough so that the shielding of the metallic vacuum chamber is not significant, the average power radiated by a Gaussian bunch of rms length σ, containing N electrons, is given by the free space result

$$\bar{P}_{\mathrm{FS}}[\mathrm{W}] = 2.42 \times 10^{-20} \frac{N^2}{R[\mathrm{m}]\rho[\mathrm{m}]} \left(\frac{\rho}{\sigma}\right)^{4/3}. \tag{10.1}$$

For longer bunches the shielding of the chamber can be approximately taken into account by using the correction factor presented in Figure 9, which was derived for an electron bunch moving on a circular orbit between parallel plates. This correction factor depends on the scaled bunch length $\Sigma = \sigma/2\rho\Delta^{3/2}$. When $\Sigma \lesssim 0.2$, $\bar{P}_{\mathrm{FS}}$ is a reasonable estimate of the coherent radiated power; however, for larger values of Σ, the shielding of the plates greatly reduces the coherent radiation.

In Table I we list the key parameters and scale factors for three storage rings. The first ring, label CSRE (Coherent Synchrotron

TABLE I

Ring	CSRE	NSLS VUV	LBL ALS
ρ [m]	0.6	1.909	4.96
R [m]	1.35	8.12	31.3
γ	293	1565	2935
σ [mm]	0.33	52.7	3.5
h [mm]	17.5	20	20
Δ	2.9×10^{-2}	1.05×10^{-2}	4.0×10^{-3}
Σ	5.5×10^{-2}	12.9	1.38

Radiation Experiment), is proposed[21] to serve as a compact, low energy ring at the NSLS with a very short electron bunch. The second ring is the NSLS VUV ring and is characteristic of an operating synchrotron light source. The third ring is the Advanced Light Source at LBL which has the shortest electron bunch for normal operations of all the existing synchrotron light sources.

For the VUV and ALS rings, Σ is too large and the bunch length is too long to observe coherent synchrotron radiation. This conclusion applies to nearly all existing electron storage rings. The CSRE ring was designed with a small bending radius and very short electron bunches to produce coherent synchrotron radiation in the millimeter portion of the spectrum. Assuming $N = 10^8$, the total coherent power radiated can be determined from Eq. (8.7) to be 15 W. More details on the coherent radiation spectrum can be found in Ref. 21.

For existing storage rings with relatively long bunches ($\Sigma > 1$), the shielding due to the plates is very important. In proposed future storage rings with short bunches ($\Sigma \ll 1$), the shielding effect will be small. The coherent radiation emission and the impedance presented to the electron beam will be close to the free space results. We believe it is of significant interest to pursue further theoretical and experimental investigations of short bunches in storage rings.

References

[1] G.A. Schott, *Electromagnetic Radiation*, Cambridge (1912) p. 168.
[2] J. Schwinger, *Phys. Rev.* **75** (1949) 1912.
[3] J.S. Nodvick and D.S. Saxon, *Phys. Rev.* **96** (1954) 180; see also L.I. Schiff, *Rev. Sci. Instr.* **17** (1946) 6.
[4] L.V. Iogansen, *Sov. Phys. JETP* **37** (1959) 299.
[5] L.V. Iogansen and M.S. Rabinovich, *Sov. Phys. JETP* **37**(10) (1960) 83; **37**(11) (1960) 856.

[6] E. Ferlenghi, *Nuovo Cimento* **48B** (1967) 73.
[7] C. Pellegrini and A.M. Sessler, *Nuovo Cimento* **53B** (1968) 198.
[8] P. Goldreich and D.A. Keeley, *Astrophysical Journal* **170** (1971) 463.
[9] A.G. Bonch-Osmolovski and E.A. Perelshtein, *Radiofizika* **13** (1970) 1089.
[10] B.G. Schinov, A.G. Bonch-Osmolovski, V.G. Makhankov and V.N. Tsytovitch, *Plasma Physics* **15** (1973) 211.
[11] A. Faltens and L.J. Laslett, *Part. Accel.* **4** (1973) 151; and in 1975 Isabelle Summer Study, BNL-20550 (1975).
[12] M. Bassetti and D. Brandt, CERN/LEP-TH/83-1 (1983).
[13] R.L. Warnock and P. Morton, *Part. Accel.* **25** (1990) 113.
[14] K.Y. Ng, *Part. Accel.* **25** (1990) 153.
[15] R.L. Warnock, SLAC PUB 5375 and 5523 (1990).
[16] S. Heifets and A. Michailichenko, *Proc. 1991 Part. Acc. Conf.* (1991) p. 458.
[17] J.B. Murphy, S. Krinsky and R.L. Gluckstern, "Longitudinal wakefield for synchrotron radiation", *Proc. 1995 Part. Accel. Conf.*, Dallas, TX, May 1995.
[18] J.D. Jackson, *Classical Electrodynamics*, Wiley, New York (1975).
[19] H. Bateman, *Higher Transcendental Functions*, Vol. II, Krieger, Malabar (1985).
[20] S.A. Kheifets and B. Zotter, CERN 95-43 (1995).
[21] J.B. Murphy and S. Krinsky, *Nucl. Instrum. Methods* **346** (1994) 571.
[22] K.Y. Ng and R.L. Warnock, *Phys. Rev. D* **40** (1989) 231.

APPENDIX A. REPRESENTATION FOR FREE SPACE IMPEDANCE

Using Eqs. (6.2) and (6.3), the impedance can be expressed in terms of the tangential electric field by

$$Z_n = -\frac{2\pi\rho^2}{ec\beta}\int_0^{2\pi} \mathrm{d}\theta\, \mathrm{e}^{-in\theta} E_\phi(\theta). \tag{A1}$$

Recall from Eq. (3.10) that the tangential electric field is a sum of the singular Coulomb field and the non-singular contribution due to synchrotron radiation. Here, we consider only the non-singular radiation field. Then for $\gamma^3 \gg 1$ and $n \gg 1$, the impedance is well approximated by

$$\frac{Z_n}{Z_0} = \frac{2\gamma^4}{3}\int_0^{\infty} \mathrm{d}\theta\, \mathrm{e}^{-in\theta} w(\mu), \tag{A2}$$

where use was made of Eq. (3.11), and $\mu = n_c\theta$ with $n_c = 3\gamma^3/2$. Also, Z_0 is the impedance of free space.

Now using Eq. (3.11) to express $w = dv/d\mu$, we carry out a partial integration in Eq. (A2) to obtain

$$\frac{Z_n}{Z_0} = \frac{4i\gamma\lambda}{9} \int_0^\infty d\mu\, e^{-i\lambda\mu} v(\mu), \tag{A3}$$

where $\lambda = n/n_c$ and $v(\mu)$ is given explicitly in Eq. (3.15). Deforming the contour of integration in Eq. (A3) from the positive real axis to the negative imaginary axis, we derive the following integral representations useful for numerical integration:

$$\begin{aligned} \mathrm{Re}\frac{Z_n}{Z_0} &= \frac{\sqrt{3}\gamma\lambda}{4} \int_1^\infty dy\, e^{-\lambda y} \frac{\left(y+\sqrt{y^2-1}\right)^{5/3} + \left(y+\sqrt{y^2-1}\right)^{-5/3}}{2y\sqrt{y^2-1}} \\ &= \frac{\sqrt{3}\gamma\lambda}{4} \int_\lambda^\infty K_{5/3}(\eta)\, d\eta, \end{aligned} \tag{A4}$$

$$\begin{aligned} &\mathrm{Im}\frac{Z_n}{Z_0} \\ &= \gamma\lambda \int_0^1 dy\, e^{-\lambda y} \frac{\left(iy+\sqrt{1-y^2}\right)^{5/3} + \left(iy+\sqrt{1-y^2}\right)^{-5/3} - 2\sqrt{1-y^2}}{4y\sqrt{1-y^2}} \\ &\quad - \gamma\lambda \int_1^\infty dy\, e^{-\lambda y} \frac{8\sqrt{y^2-1} - \left(y+\sqrt{y^2-1}\right)^{5/3} + \left(y+\sqrt{y^2-1}\right)^{-5/3}}{8y\sqrt{y^2-1}}. \end{aligned} \tag{A5}$$

The results of the numerical integration are shown in Figure 5, and confirm the asymptotic forms given in Eqs. (6.18) and (6.20).

Having accomplished our goal of deriving Eqs. (A4) and (A5), let us close with the following comment. Since the wakefield vanishes behind the point charge, the Kramers–Kronig relations hold, and the wakefield can be expressed in terms of the real part of the impedance. One can show that for $\mu > 0$

$$w(\mu) = \frac{9\sqrt{3}}{8\pi} \int_0^\infty d\lambda\, (\cos\mu\lambda)\lambda \int_\lambda^\infty d\eta\, K_{5/3}(\eta), \tag{A6}$$

which expresses the wakefield as a cosine transform of Schwinger's[2] result for the frequency spectrum of synchrotron radiation. Also note that Eq. (A6) could be derived starting from Schott's result of Eq. (2.16), taking the large γ limit, and converting the sum over m to an integral, after approximating the J-Bessel functions in terms of K-Bessel functions.

APPENDIX B. APPROXIMATE IMPEDANCE DERIVED FROM THE SCALED WAKEFIELD FUNCTION G_2

The wakefield due to synchrotron radiation can be approximated from Eq. (5.21) as

$$E_\phi \simeq E_\phi^{\mathrm{FS}} + \frac{e}{2\rho^2\Delta^2} G_2(\xi/\Delta^{3/2}), \tag{B1}$$

where the first term is the free space contribution and the second term contains the dominant contribution of the parallel plates wakefield which satisfies the scaling law given in Section 5.

It should be noted that the exact parallel plate wakefield contains a small contribution which does not satisfy the scaling law and is not included in Eq. (B1). As such the approximate impedance considered in this appendix can be expected to have different analytic properties from the exact impedance.

Using Eq. (B1) in Eq. (A1), and recalling $\theta = 2\xi$, we derive

$$Z_n \simeq Z_n^{\mathrm{FS}} - \frac{Z_0}{2\Delta^{1/2}} \int_{-\infty}^{\infty} \mathrm{d}x\, \mathrm{e}^{-2in\Delta^{3/2}x} G_2(x), \tag{B2}$$

denoting the free space impedance Z_n^{FS}. Utilizing the expression for G_2 given in Eq. (5.22b), and the retardation condition of Eq. (5.9), we write

$$G_2(x) = 4 \sum_{k=1}^{\infty} \frac{(-1)^{k+1}}{k^{1/2}} \frac{\mathrm{d}}{\mathrm{d}x} \left(\frac{y_k^3}{1+y_k^4} \right). \tag{B3}$$

Inserting this in Eq. (B2) yields

$$Z_n \simeq Z_n^{\mathrm{FS}} - 4iZ_0 n\Delta \sum_{k=1}^{\infty} \frac{(-1)^{k+1}}{k^{1/2}} \int_{-\infty}^{\infty} \mathrm{d}x\, \mathrm{e}^{-2in\Delta^{3/2}x} \frac{y_k^3}{1+y_k^4}. \tag{B4}$$

We now use Eq. (5.9) to change the integration variable from x to y_k, obtaining

$$Z_n \simeq Z_n^{\mathrm{FS}} - 2iZ_0 n\Delta \sum_{k=1}^{\infty} (-)^{k+1} k \int_0^{\infty} y\,\mathrm{d}y \exp\left[-in(\Delta k)^{3/2}\left(\frac{y^3}{3} - \frac{1}{y}\right)\right]. \tag{B5}$$

Changing the integration variable to v, defined by

$$y = \frac{3^{1/3}\mathrm{e}^{-i\pi/6} v}{n^{1/3}(\Delta k)^{1/2}}, \tag{B6}$$

we derive

$$Z_n \simeq Z_n^{\mathrm{FS}} - 2iZ_0 n^{1/3}\mathrm{e}^{-i\pi/3} 3^{2/3} \sum_{k=1}^{\infty} (-1)^{k+1} \int_0^{\infty} v\,\mathrm{d}v \exp\left(-v^3 - \frac{\alpha^2 k^2}{2v}\right), \tag{B7}$$

where we have introduced

$$\alpha^2 \equiv \frac{2\mathrm{e}^{-i\pi/3} n^{4/3}\Delta^2}{3^{1/3}}. \tag{B8}$$

Consider the sum

$$S \equiv \sum_{k=1}^{\infty} (-1)^{k+1} \mathrm{e}^{-\alpha^2 k^2/(2v)} = \frac{1}{2} + \frac{1}{2} \sum_{k=-\infty}^{\infty} (-1)^{k+1} \mathrm{e}^{-\alpha^2 k^2/(2v)}. \tag{B9}$$

Using the Fourier expansion

$$\mathrm{e}^{-\alpha^2 k^2/(2v)} = \int_{-\infty}^{\infty} \mathrm{d}t \frac{v^{1/2}}{\sqrt{2\pi}\alpha} \mathrm{e}^{ikt} \mathrm{e}^{-vt^2/(2\alpha^2)} \tag{B10}$$

together with the Poisson summation formula

$$\sum_{m=-\infty}^{\infty} \delta(t - (2m+1)\pi) = \frac{1}{2\pi} \sum_{k=-\infty}^{\infty} (-)^k \mathrm{e}^{ikt}, \tag{B11}$$

it is seen that

$$S = \frac{1}{2} - \sqrt{\frac{\pi v}{2}} \frac{1}{\alpha} \sum_{m=-\infty}^{\infty} \exp\left[\frac{-v\pi^2(2m+1)^2}{2\alpha^2}\right]. \tag{B12}$$

Transforming the sum in Eq. (B7) by using Eq. (B12), we derive

$$Z_n \approx Z_n^{\mathrm{FS}} - \frac{Z_0\Gamma(2/3)}{3^{1/3}}\left(\frac{\sqrt{3}}{2} + \frac{i}{2}\right)n^{1/3} + 2e^{i\pi/6}Z_0 3^{2/3} n^{1/3} \frac{\sqrt{2\pi}}{\alpha} \sum_{p(\mathrm{odd})=1}^{\infty} h\left(\frac{\pi^2 p^2}{2\alpha^2}\right), \tag{B13}$$

with the function $h(z)$ defined by

$$h(z) = \int_0^{\infty} v^{3/2}\, dv\, e^{-v^3 - zv}. \tag{B14}$$

The expression for the impedance given in Eq. (B13) is in the appropriate form to compare with the results of Section 7. In particular, the summation over image charges k has been converted to a sum over waveguide modes p.

The approximate expression for $\mathrm{Re}\, Z_n$ given in Eq. (7.9) can be derived from Eq. (B13) by carrying out an asymptotic approximation of $h(z)$ for large z (i.e. small $n \ll [\pi/(2\Delta)]^{3/2}$), using the method of steepest descent.

The saddle point analysis proceeds as follows: Let

$$\alpha = a e^{-i\pi/6}, \quad a = \frac{\sqrt{2} n^{2/3} \Delta}{3^{1/6}},$$

$$z = \hat{z} e^{i\pi/3}, \quad \hat{z} = \frac{\pi^2 p^2}{2a^2}.$$

For $n \ll 3\gamma^3/2$, the first two terms of Eq. (B13) cancel, and

$$Z_n = \frac{2Z_0 3^{2/3} n^{1/3} \sqrt{2\pi}}{a} \sum_{p(\mathrm{odd})=1}^{\infty} e^{i\pi/3} \int_0^{\infty} v^{3/2}\, dv \exp\left[-v^3 - \hat{z} e^{i\pi/3} v\right]. \tag{B15}$$

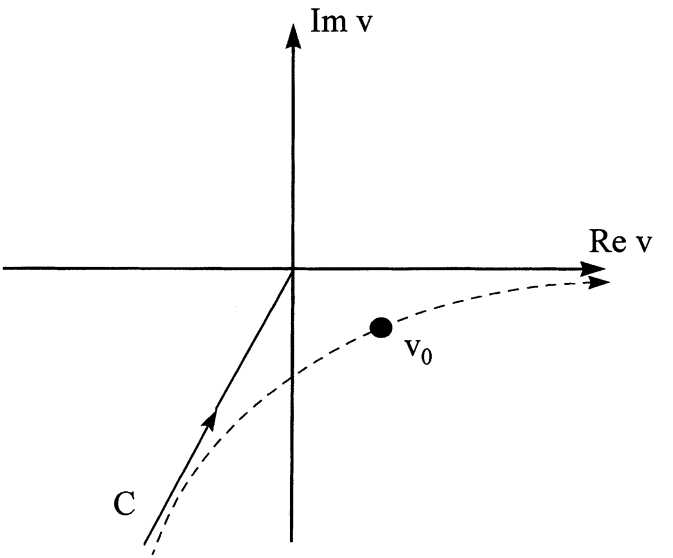

FIGURE 11 Contour C utilized in the integral of Eq. (B16), and the distorted contour through the saddle point v_0.

The real part of Z_n is given by

$$\begin{aligned}
\operatorname{Re} Z_n &= \frac{1}{2}(Z_n + Z_n^*) \\
&= \frac{Z_0 3^{2/3} n^{1/3} \sqrt{2\pi}}{a} \sum_{p(\text{odd})=1}^{\infty} \left[e^{i\pi/3} \int_0^{\infty} v^{3/2}\, dv\, \exp(-v^3 - \hat{z} e^{i\pi/3} v) \right. \\
&\quad \left. + e^{-i\pi/3} \int_0^{\infty} v^{3/2}\, dv\, \exp(-v^3 - \hat{z} e^{-i\pi/3} v) \right] \\
&= \frac{Z_0 3^{2/3} n^{1/3} \sqrt{2\pi}}{a} \sum_{p(\text{odd})=1}^{\infty} \left[e^{i\pi/3} \int_0^{\infty} v^{3/2}\, dv\, \exp(-v^3 - \hat{z} e^{i\pi/3} v) \right. \\
&\quad \left. + e^{i\pi/3} \int_{\infty e^{-2\pi i/3}}^{0} v^{3/2}\, dv\, \exp(-v^3 - \hat{z} e^{i\pi/3} v) \right] \\
&= \frac{Z_0 3^{2/3} n^{1/3} \sqrt{2\pi}}{a} \sum_{p(\text{odd})=1}^{\infty} e^{i\pi/3} \int_C v^{3/2}\, dv\, \exp(-v^3 - \hat{z} e^{i\pi/3} v),
\end{aligned} \tag{B16}$$

where the contour C is shown in Figure 11.

For $\hat{z} \gg 1$, i.e. $n \ll [\pi/(2\Delta)]^{3/2}$, the contour integral in Eq. (B16) can be approximated by a steepest descent analysis. We define

$$f(v) = v^3 + \hat{z}e^{i\pi/3}v. \tag{B17}$$

The saddle point v_o satisfies $f'(v_o) = 0$. We choose

$$v_0 = \frac{\pi p}{a\sqrt{6}}e^{-i\pi/3}. \tag{B18}$$

In this case

$$f(v_0) = \frac{2}{3}\left(\frac{\pi p}{2\Delta}\right)^3 \frac{1}{n^2}, \tag{B19}$$

$$f''(v_0) = \frac{\pi p\sqrt{6}}{a}e^{-i\pi/3}. \tag{B20}$$

Deforming the contour C to follow the path of steepest descent through the saddle point, we find

$$\mathrm{Re}\, Z_n \simeq \frac{Z_0 3^{2/3} n^{1/3}\sqrt{2\pi}}{a}e^{-i\pi/3}\sum_{p(\mathrm{odd})=1}^{\infty} v_0^{3/2}e^{i\pi/6}\sqrt{\frac{2\pi}{|f''(v_0)|}}e^{-f(v_0)}, \tag{B21}$$

which leads to the final result for $n \ll [\pi/(2\Delta)]^{3/2}$:

$$\mathrm{Re}\, Z_n \simeq \sum_{p(\mathrm{odd})=1}^{\infty} \frac{Z_0\pi^2 p}{2n\Delta^2}\exp\left[-\frac{2}{3}\left(\frac{\pi p}{2\Delta}\right)^3\frac{1}{n^2}\right]. \tag{B22}$$

Due to the neglect of the non-scaling part of the wakefield, the approximate impedance considered in this appendix has different analytic properties than the exact impedance of Eq. (7.1). The exact impedance has branch points at the cutoff frequencies, $n = p\pi/2\Delta$ ($p = 1, 3, 5, \ldots$) and is analytic[22] about the origin $n = 0$. The exact impedance is pure imaginary on the real n-axis for $|n| < \pi/2\Delta$. The approximation to the impedance considered here does not exhibit the branch points at the cutoff frequencies, and has an essential singularity at the origin as indicated in Eq. (B22). For $n > \pi/2\Delta$, the real part

of the exact impedance behaves as shown in Eq. (7.9), which is identical to Eq. (B22). In the case of the exact impedance, the essential singularity at the origin is located on the second Riemann sheet, not the first, and can only be reached by analytically continuing across the branch cut.

APPENDIX C. NUMERICAL ILLUSTRATION OF THE SCALING PROPERTY OF THE PARALLEL PLATE WAKEFIELD

To explore the scaling properties of the parallel plate wakefield we examine the contributions to it of the functions $V_{2,k}$ given in (5.3b). Since we are looking for the effect of the plates, we ignore the free space contribution ($k=0$) and consider the following:

$$E_2^{\mathrm{pp}}(\xi) = -\frac{e\beta^2}{2\rho^2}\sum_{\substack{k=-\infty \\ k\neq 0}}^{\infty}(-1)^k\frac{\partial V_{2,k}(\xi)}{\partial\xi} = \frac{4e\beta^2\gamma^4}{3\rho^2}\sum_{k=1}^{\infty}(-1)^{k+1}W_{2,k}(\xi), \quad \text{(C1)}$$

where

$$W_{2,\mathrm{k}}(\xi) \equiv \frac{3}{4\gamma^4} \times \frac{(s_k^2 - \beta s_k \sin[2\alpha_k]/2)\sin[2\alpha_k] - \sin^2[\alpha_k](\sin[2\alpha_k]/2 - s_k\beta\cos[2\alpha_k])}{[s_k - \beta\sin[2\alpha_k]/2]^3},$$

$s_k = \sqrt{\sin^2\alpha_k + (k\Delta)^2}$ and ξ is a solution of the retardation equation (5.5)

Numerically solving Eq. (5.5), we evaluate

$$W_2(\xi) \equiv \sum_{k=1}^{25}(-)^{k+1}W_{2,k}(\xi)$$

and the results are given in Figures 12–14 for the three values of the parameter $\Delta = 10^{-1}$, 10^{-2} and 10^{-3}, respectively, assuming $\gamma = 300$ and including 25 terms in the sum over k in (C1). It can readily be seen from the figure that the curves differ only in the scaling of the

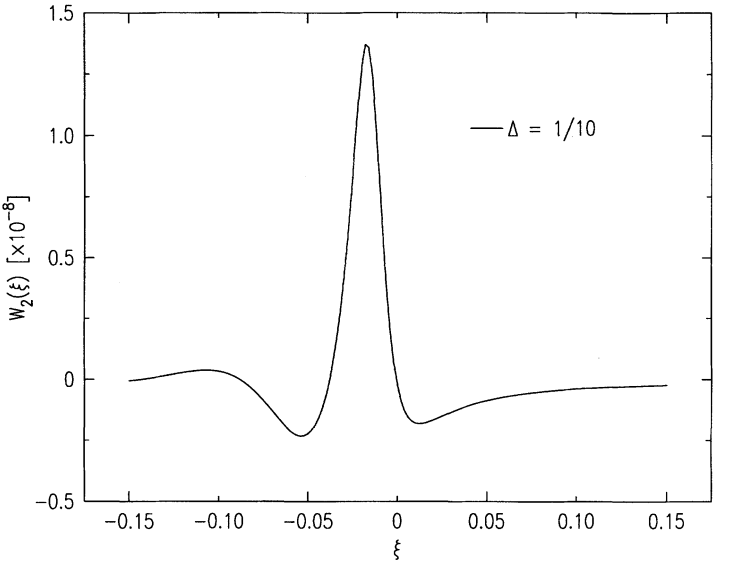

FIGURE 12 Plot of W_2 (ξ) as given in Eq. (C1) versus ξ for $\Delta = 10^{-1}$, assuming $\gamma = 300$ and including 25 terms in the sum over k.

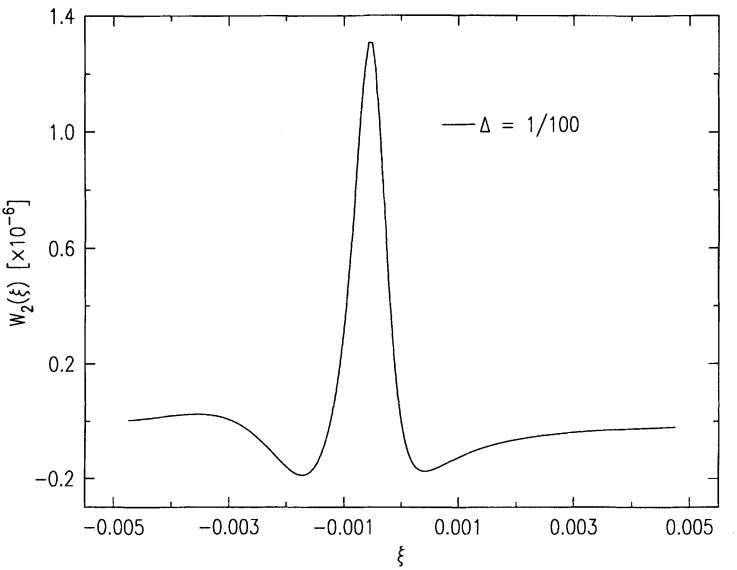

FIGURE 13 Plot of W_2 (ξ) as given in Eq. (C1) versus ξ for $\Delta = 10^{-2}$, assuming $\gamma = 300$ and including 25 terms in the sum over k.

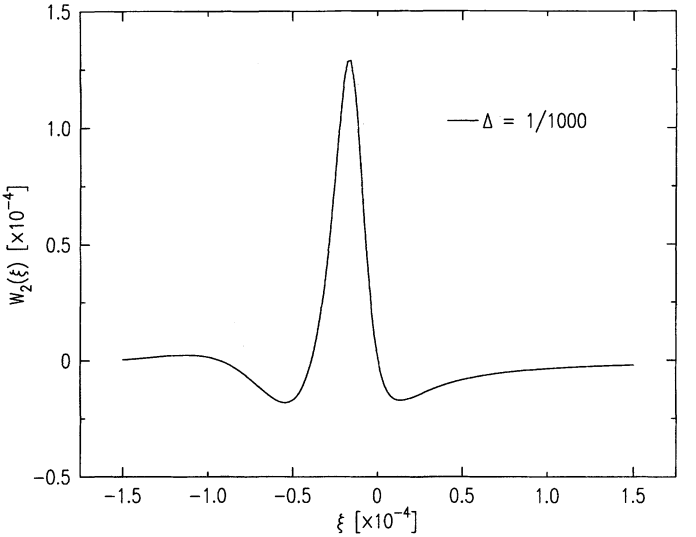

FIGURE 14 Plot of $W_2(\xi)$ as given in Eq. (C1) versus ξ for $\Delta = 10^{-3}$, assuming $\gamma = 300$ and including 25 terms in the sum over k.

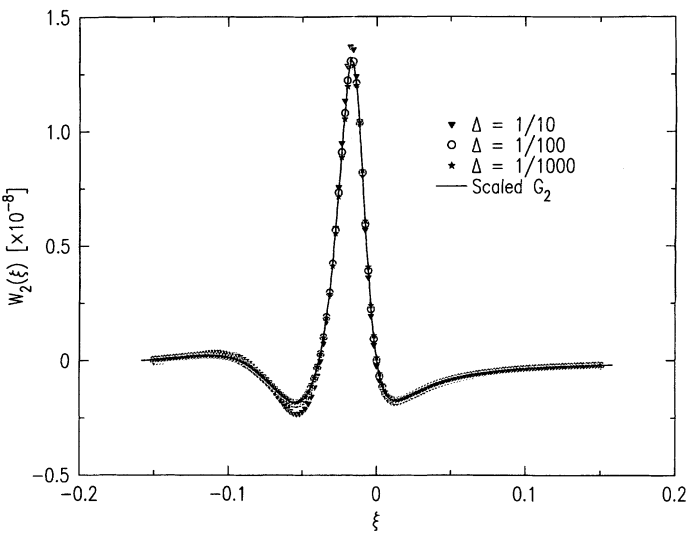

FIGURE 15 Plot of $W_2(\xi)$ versus ξ for $\Delta = 10^{-1}$, 10^{-2}, and 10^{-3} as given in Figures 12–14. The data for $\Delta = 10^{-2}$ and 10^{-3} have had the vertical axes scaled by Δ^{-2} and the horizontal axes by $\Delta^{3/2}$. Also included in the figure is the function $[3/(8\Delta^2\gamma^4)]G_2(\xi/\Delta^{3/2})$ scaled to $\Delta = 10^{-1}$.

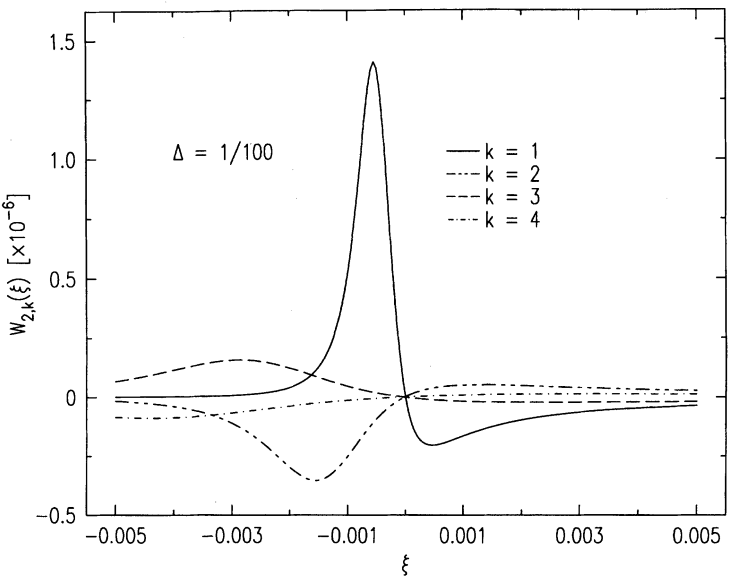

FIGURE 16 Plot of $W_{2,k}(\xi)$ as given in Eq. (C1) versus ξ for $\Delta = 10^{-2}$, $\gamma = 300$ and $k = 1$–4.

vertical axis by Δ^{-2} and the horizontal axis by $\Delta^{3/2}$. The scaling behavior is displayed graphically in Figure 15 where the data for $\Delta = 10^{-2}$ and 10^{-3} are scaled as noted and plotted on the same set of axes as the $\Delta = 10^{-1}$ data, along with the function $[3/(8\Delta^2\gamma^4)]G_2(\xi/\Delta^{3/2})$ (Eq. (5.22)) scaled for $\Delta = 10^{-1}$. It can be seen that all the numerical results are well approximated by the scaling curve derived from G_2. These results are valid as long as $\gamma^2\Delta \gg 1$.

While the sum over k in Eq. (C1) extends to infinity, there is a rapid convergence with increasing k if we restrict ourselves to the region $|\xi| \leq \Delta$. This is demonstrated numerically in Figure 16 for $\Delta = 10^{-2}$, where we plot $W_{2,k}(\xi)$ versus ξ for $k = 1$–4. This rapid convergence in the region $|\xi| \leq \Delta$ shows that the sum is dominated by only a few leading terms in the series of Eq. (4.8).

A similar analysis can be carried out for the $V_{1,k}$ contribution to the wakefield and the G_1 scaling function, and quick convergence is also observed in this case.